UNIVERSITY OF EDUCATION, WINNEBA

COLLEGE OF TECHNOLOGY EDUCATION - KUMASI

THE EFFECT OF COOLING RATE ON THE MECHANICAL PROPERTIES OF CARBON STEEL ON WELDED JOINTS

GLADYS PERPETUAL AWUDI

200029535

NOVEMBER, 2021

UNIVERSITY OF EDUCATION, WINNEBA

COLLEGE OF TECHNOLOGY EDUCATION - KUMASI

THE EFFECT OF COOLING RATE ON THE MECHANICAL PROPERTIES OF CARBON STEEL ON WELDED JOINTS

GLADYS PERPETUAL AWUDI

200029535

A Thesis in the Department of Mechanical and Automotive Technology Education, Faculty of Technical Education, Summited to the School of Graduate Studies, University of Education, Winneba in partial fulfilment of the Requirement for the Award of Master of Philosophy (Mechanical Engineering Technology) Degree

NOVEMBER, 2021

DECLARATION

Student's Declaration

I, Gladys Perpetual Awudi declares that this Thesis with the exception of the quotations and references contained in the published work which have all been identified and duly acknowledged, is entirely my own original work and it has not been submitted either in part or whole for another degree elsewhere.

Signature: …….

Date: ……..

Supervisor's Declaration

I hereby declare that the preparation and presentation of this work was supervised in accordance with the guidelines for supervision of thesis as laid down by the University of Education, Winneba.

Name of Supervisor: Dr. Kwabena Offeh Gyimah

Signature: …….

Date: ……..

ACKNOWLEDGEMENT

I am very grateful to the Most High God for seeing me through yet another stage in my life. Without Him, this would have been impossible.

I am also grateful to my supervisor, Dr. Kwabena Offeh Gyimah, a Lecturer at the Department of Mechanical and Automotive Technology Education, College of Technology Education Kumasi, University of Education, Winneba whose guidance, advice and support led to the success of this research work. To Dr. Ing. Enock A. Duodu, Head, Department of Mechanical and Automotive Technology Education, College of Technology Education, Kumasi, University of Education, Winneba, your great leadership, support and pieces of advice were of immense help to me. I am grateful.

My sincerest appreciation goes to the management and staff of Tema Steel Company, especially Engr. Royal, Engr. King Solomon, Mr. Samuel, Gladstone Tettey and all the Technicians who assisted me in preparing the specimen for this work. I am most grateful to Very Rev'd Dr. John Abedu Quashie (Senior Lecturer, Trinity Theological Seminary) for all the encouragement and support.

To Engr. Joseph Nyumutsu and his team at the Kwame Nkrumah University of Science and Technology (KNUST) where I did the test for this work, I am very grateful for your assistance. To Mr. Ebenezer Nunoo, Mr. Philip Duagbo Quarshigah, Mr. Kobina Otu Okyne, your support is greatly appreciated.

I am equally grateful to Mr. Yussif Atta, Laboratory Technician at the Koforidua Technical University, Faculty of Engineering, Mechanical Department, you are more than a colleague, God bless you for all your effort. To Mr. Philip Adu Takyi and Isaac Tetteh of the Solutions Department of the Design and Technology Institute (DTI), guys, you are amazing. God bless you all for being a part of this.

DEDICATION

I dedicate this work to the Triune God for seeing me through this work, especially when all hope was lost.

Thank you Lord for your grace, love, provision and above all, peace. Indeed, your peace surpasses all understanding.

I also dedicate this to my mum and dad, all of blessed memory.

Mum, you were looking forward to this day.....

Dad, your Baby girl did it by God's grace!

TABLE OF CONTENT

CONTENT **PAGE**

LIST OF FIGURES

LIST OF TABLES

ABSTRACT

AISI 1028 Low carbon steel is a type of steel that contains 0.05% to 0.25% of carbon, Its easiness to cut, form, weld and its excellent mechanical properties makes it very useful in numerous industrial activities. It is the least expensive of the carbon steels to produce and buy. This makes it the preferred steel for manufacturing auto parts, pipelines, and for ornamental uses like gates and fences for homes and businesses. This study has become very necessary because of the current economic situation in the country, making most of the welders using scrap metals instead of the new ones for fabrication and construction works. The specific objectives of this study is to evaluate the effects of cooling rate on new and scrap carbon steel metals on welded joints by the Manual Metal Arc Welding Process and to appraise the effects of the cooling rate on the mechanical properties of the welded joints using experimental and analytical methods. The heat treated welded samples were cut and machined to standard configurations for tensile strength, hardness and impact test. The results showed that there are significant effect of heat treatment on the hardness, tensile strength and impact energy of both the new and scrap carbon steel. The results indicated that the new low carbon steels were 3.10%, 5.55% and 28.94% harder than the scrap carbon steel when cooled in water, air and oil respectively. It also proves that the ultimate strength of new low carbon steel were 38.91%, 38.40% and 42.75% and its elasticity 31.95%, 64.88% and 46.78% higher than the scrap carbon steel when cooled in water, air and oil respectively. However, when the impact energy values were considered, the scrap carbon steel had higher impact energy of 54.55%, 32.14% and 35.78% as compared to the new carbon steel.

CHAPTER ONE

INTRODUCTION

1.1 Background to the Study

Welding is a very vital process in production due to the high joint efficiency, flexibility, simple set up and the low cost of fabrication. It is an efficient, reliable and economical process. Welded joints are key in any construction sector, and if there should be any failures, it can be very dangerous. Hence, standards must be taken seriously with keen interest in precision quality. This can be achieved if we can control mainly the heat input and effects that the cooling rate has on the welded joint Chryssolouris (2013).

This research seeks to analyse the effect of cooling rate on mechanical properties of carbon steel (both new and recycled) welded joints. The specimens will be prepared to apply to tensile, torsion, impact and hardness tests. The prepared specimens which will be heat treated at (850 ^{0}C) for one hour and subsequently cooled by three different media (Water-Air-furnace) to show the effect of Medias cooling rate on mechanical properties. The microstructures of all specimens will be examined before and after heat treatment by an optical microscope. To determine the phases obtained after heat treatment and its effect on the mechanical and corrosion properties. The experimental results will indicate whether the microstructure of steel can be changed and significantly improved by varying line cooling rate thus, improving one property will have an effect on the others because of the relationship between all properties.

Many industrial applications of heat conduction, such as continuous castings, welding, extrusion, anti-icing etc., involve solidification or melting with phase change. Heat conduction problems involving solidification and melting are also regarded as the Stefan problems. Generally, the Stefan problems are non-linear, due to the presence of the moving

boundary whose position is not known a priori, Petrus et al. (2010). Pioneering work on such problems dates back to Evans et al. (2010), in which they analysed the exact solutions of such problems. Since then, there has been a tremendous focus on numerical solution of the Stefan problems.

Rubinstein (2011) proposed a complex mathematical model to solve the Stefan problem. This model was based on an interface that moves either into the solid region (melting) or into the liquid region (solidification), in accordance with the relative magnitude of temperature gradients on either sides of the interface. Due to the complex nature of the model, the applicability of this model was limited to one-dimensional problems only.

Bonacina (2013) proposed a three-time level implicit fixed mesh approach, which was unconditionally stable and convergent. This scheme was based on an analytical approach consisting of an approximation of the latent heat by a large heat capacity over a small range of temperature. In this approach, temperature dependent coefficients were evaluated at intermediate time level; therefore, the complication of solving a set of non – linear equations at every time step was avoided. However, this method was limited to problems with a small interval of temperature, over which solidification takes place and also deals with a drawback of severe nonlinearity in material property.

Bonnerot and Janet (2007) used a time-variant mesh approach to solve a phase change problem involving heat conduction only. In this explicit scheme, the mesh was deformed dynamically so that a continuous track of the solid/liquid front location could be achieved. This method offered high accuracy; however, it was limited to simpler problems and geometries, with the drawback of large computational time. Gartling (2007) approached both the free and forced convection phase change problems by using temperature dependent properties based on a finite element method. In this method, field equations

were discretized using Galerkin method. In the current study, NACHOS H developed by Gartling (2007) and modified by Amin and Greif (2009) was used as a starting point.

Morgan et al. (2008) simplified and improved the previously mentioned work of Bonacina et al. (2013) by reconsidering the latent heat effect accompanied by a phase change. In this approach, the latent heat effect accompanied by a phase change was approximated by integration of the terms involving heat capacity. Therefore, it required an accurate evaluation of heat capacity at integration points. Their results led to an important finding that the time step size should not exceed the temperature interval over which solidification takes place.

The focus of study by Jaluria (1983) associated with a continuously moving material undergoing thermal processes was the thermal buoyancy, transient, and forced flow in the ambient medium. Three main approaches were outlined in this work. The first was directed at the heat transfer in the material, assuming convective coefficients at the surface. The second solved for the flow generated by an isothermal-moving surface. The third approach was the combination of the above two that considered the conjugate problem that couples the flow and transport in the fluid with those of the material.

The investigations of Huang et al. (1992) on superheated dissipation in the CC process revealed that most of the heat is dissipated in the mould or just below the mould. Also, the amount of superheat and casting speed were found to be the dominating factors. The investigations on two-dimensional mathematical models, which included the effects of nozzle jet angle and submergence depth on the shell thickness and heat flux, were able to predict many three-dimensional results.

Lee and Tzong (1995) presented a modified latent heat method for a binary alloy system by solving species and momentum equations in the liquid and the mushy zones. In this method, an interpolation technique was proposed to trace the interface of the mushy zone and the pure liquid region. The results obtained by this technique revealed that a great amount of latent heat could be released from an area when the eutectic front sweeps through it. Furthermore, the total volume of the mushy zone predicted by this method showed a satisfactory agreement with the experimental results.

Lee and Chiou (2015) developed an average specific heat method to simulate the properties of the elements undergoing the phase change, which was later used by Greif (1998) in the conjugate heat transfer in a continuously moving metal during solidification. This method was found to have little effect of the time step on the average and maximum error. Therefore, larger time steps could be used in this method to save computational time. Insensitivity towards the temperature interval over which the solidification takes place was another advantage of this method. The present study of CC process is based on this method.

Although numerical analyses of coupled fluid and heat transfer in the CC process date back almost two decades, only a few studies have been aimed at coupled turbulent flow and heat transfer with solidification in pure metal CC process.

Brimacombe et al. (1991) approached the phenomenon of CC castings by the heat transfer aspect of the process alone. In this approach, the authors used an equation similar to a conduction equation with a relatively large thermal conductivity in the liquid pool region to account for possible effects of turbulence on the heat transfer.

The experimental study of Nakato et al. (1981) was aimed at the factors affecting the formation of shell and longitudinal cracks. Their experiments indicated that the withdrawal speed, stream velocity from the submerged nozzle, mould taper and mould oscillations were influential factors in the shell formation. They also found that the casting speed and the mould powder are the most influential factors to the mean heat flux in the mould. This research work would analyse the effects of cooling rate on new and used scrap carbon steel metals on welded joints.

1.2 Statement of the Problem

A technique to prevent solidification cracking is required in the welding process, because stainless steels, nickel-based super alloys and dissimilar welded joints are susceptible to this phenomenon. Solidification cracking becomes a more serious problem when different materials and an increased welding speed are used for the high functionalization of the mechanical structure and to increase productivity (Dupont, Lippold, & Kiser, 2011). Optimization of the welding joint design and development of the welding material have been attempted to prevent the occurrence of solidification cracks. However, a definite prevention technique for solidification cracking has not yet been developed. Thus, it is necessary to analyse both the solidification phenomenon and distribution of loaded strain during welding in detail, and to elucidate the mechanism of the solidification cracking phenomenon. This research work was done to analyse the effects of cooling rate on the mechanical and corrosion properties of new and used scrap carbon steel metals on welded joints.

1.3 Purpose of the Study

The aim of the study was to analyse the effects of cooling rate on new and used scrap carbon steel metals on welded joints and to know the effects of this cooling rate on the mechanical and corrosion properties of the welded joints. This has become very necessary because of the current economic situation in the country, making most of the welders using scrap metals instead of the new ones for fabrication and construction works.

1.4 Specific Objectives

The following specific objectives were formulated to guide the study:

i. To evaluate the effects of cooling rate on welded joints of new carbon steel plates by the Manual Metal Arc Welding Process.
ii. To evaluate the effects of cooling rate on welded joints of scrap carbon steel plates by the Manual Metal Arc Welding Process.
iii. To appraise the effects of the cooling rate on the mechanical properties of the welded joints of both new and scrap metal plates.

1.6 Organization of the Thesis

The entire study was divided into five chapters. Chapter One dealt with the introduction. It included the background to the study, statement of the study, purpose of the study, objective of the study, the methods and materials used, and the organization of the study. Chapter Two reviewed related literature about scrap metals, the effects of solidification rate of new carbon steels and scrap metals on the fabricated artefacts. Chapter Three focused on the materials and methods used to conduct the study as well as methods used for data analysis. Chapter Four dealt with the analysis of results and discussion. Chapter Five focused on the summary of the results, conclusions, recommendations and suggestions for future research.

CHAPTER TWO

LITERATURE REVIEW

2.1 Introduction

This chapter comprehensively reviewed literature on the effect of cooling rate on the mechanical and corrosion properties of carbon steel welded joints. We looked at recycled or scrap metals, the effects of cooling rate of carbon steels on the welded joint, the microstructure of carbon steel, the microstructural phases, solidification of carbon steels, the solidification process in carbon steels **etc.**

2.2 Recycle or Scrap steel

Steel is perhaps the most important construction material in the world, providing services for the well-being of mankind. An increased demand for steel services creates demand for steel consumption, and the lifetime of the products in use determines the recycling potential and the need for replacement. At the same time the steel sector contributes 9 % to global energy consumption and process-related carbon emissions. This is a figure that is very much dependent on the amount of steel recycled, because production of steel from recycled material can be carried out with much less energy and CO_2 emissions.

Considering volume, steel is already the most recycled metal, and there is a well-functioning business structure for the recycling of steel. Currently about 40% of the steel produced comes from recycled material. If and when the increase in world consumption of steel decreases, there will be numerous possibilities of producing a large amount of the steel from recycled scrap.

Based on the existing process technology for scrap sorting and steel processing and on what is known about scrap quality, possible limitations and possible actions, the chapter discusses possibilities to reach a truly sustainable steel recycling. The greatest challenge for the steel and scrap processing industry to obtain long term sustainable steel recycling is perhaps the question of scrap quality and the need to avoid quality losses when recycling steel. As the share of steel produced from ore has increased in the last decade, accumulation of tramp elements has not been an issue of high importance recently, but it is an issue that has to be tackled in the future (Markus Reuter, Ernst Worrell 2014).

Steel is everywhere in our lives and is at the heart of a sustainable future. The steel industry is an integral part of the global circular economy. The circular economy is a move from linear business models, in which products are manufactured from raw materials and then discarded at the end of their useful lives, to circular business models where intelligent design leads to products or their parts being repaired, reused, returned and recycled (Broadbent, 2016).

A circular economy aims to rebuild capital, whether it is financial, manufacturing, human, social or natural. This approach enhances the flow of goods and services (Broadbent, 2016). The concept of the circular economy drives optimal resource efficiency. It makes sure that resources are efficiently allocated to products and services in such a way as to maximise the economic well-being of everyone. In addition, products need to be designed to be durable, easy to repair and, ultimately, to be recycled. The cost of reusing, repairing or remanufacturing products has to be competitive to encourage these practices. Simply replacing a product with a new one should no longer be the norm.

A circular economy ensures that value is maintained within a product when it reaches the end of its useful life while at the same time reducing or eliminating waste. This idea is fundamental to the triple-bottom-line concept of sustainability, which focuses on the interplay between environmental, social and economic factors. In a well-structured circular economy, the steel industry has significant competitive advantages over competing materials and these can be demonstrated through a life cycle approach.

Life cycle assessment in the steel industry

The World Steel Association (worldsteel) has been developing a database of life cycle inventories (LCI) of steel products for more than 20 years together with an externally reviewed methodology report. This LCI database of 15 steel products accounts for the cradle to gate steel production, including raw material mining and manufacturing, as well as accounting for the benefits of recycling steel from products at the end of their life. This database and methodology assist LCA practitioners modelling steel products to carry out full cradle to grave life cycle assessments.

Steel recycling practice

In the manufacture of steel, the term ‘primary production’ generally refers to the manufacture of iron (hot metal) from iron ore in a blast furnace (BF), which is subsequently processed in the basic oxygen furnace (BOF) to make steel. ‘Secondary production’ refers to the ‘recycling’ route and is typically the electric arc furnace (EAF) process, which converts scrap into new steel by re-melting old steel. However, primary steel production is not unique to the BOF route, and similarly, secondary steel production is not unique to the EAF. It is common practice to use 10–30 % scrap as iron input in the

BOF route. Primary steel production also occurs in the EAF route, when pre-reduced iron is used as a feedstock to the EAF process (Lee et al. ,1996)

Steel is 100 % recyclable and scrap is converted to the same (or higher or lower) grade steel depending upon the metallurgy and processing of the required product. Some recycled products such as rebar require minimal processing, whilst the higher value engineering steels require more metallurgical and process controls to meet tighter specifications. The final economic value of the product is not determined by recycled content, and there are many examples of high value products that contain large amounts of recycled steel. Some steel products are principally sourced via the primary route mainly because the steel specifications require low residual elements and this can be achieved most cost-effectively using more primary material. In most cases, scrap with a low amount of residual elements commands a higher market price owing to the ease of processing through the recycling routes (Broadbent, 2016).

The growing global demand for steel results in a continuing capacity to absorb steel scrap. There is not enough scrap arising to manufacture all the steel required to satisfy the market. This is not a consequence of deficiencies in collecting scrap as the recovery rates of steel products are high and the lifetime of products is often long. Moving towards a circular economy, if more scrap becomes available, this could result in an increase in the proportion of steel made in the EAF route. Continuing improvements in the scrap processing plants and segregation of scrap types will improve efficiencies in the steel-making process (Pauliuk2017).

2.3 Effects of cooling rate of carbon steels on the welded joint

Recently, numerous studies about temperature evolution, cooling rate, residual stresses and distortion, among others have been developed through parametric and empirical modelling. Allazadeh (2012) predicted the strain and residual stress evolution within a geometrically complex specimen (cylinder, cones, spheres,) dealing with estimation of microstructure and hardness distribution after quenching using a mathematical method based on the finite volume method to test for existence or formation of anomalies or defects before or after quenching.

A quenching simulation for more complex geometry such as stepped cylinder and axially symmetric steel work piece were developed by other programmers. Hömberg (2016) developed the model of a quenching process to study the effect of actual service condition aspects such as the presence of holes or notches using temperature dependent materials properties. Bhadeshia (2010) extended Johnson-Mehl-Avrami-Kolmogorov model to study two linearly dependent precipitation isothermal reactions. Reti et al. (2001), developed a phenomenological kinetic model flexible for both isothermal and non-isothermal conditions to describe the multiphase diffusional austenite decomposition which occurs during quenching of low alloy hypo eutectoid steel after austenization through pseudo-autonomous differential equations. This model was used to determine the hardness in a bar for a specific composition and diameter, which the agreement between numerical and experimental results was very well.

Xin (2017) researched on the effect of heat treatment on microstructure and hardness of internal crack healing in a low carbon steel. The internal cracks were produced into the samples by a drilling and compression method. The microstructure of crack healing zone was examined using optical microscopy (OM) and scanning electron microscopy (SEM).

The hardness of crack healing zone was measured using a Vickers micro-hardness testing machine (FM-800). The results show that healing temperature plays a more significant role in internal crack healing than holding time. Compared as-quenched samples with as-normalized samples under the same healing parameters, it is found that cooling speed is also an important factor for internal crack healing. The migration and enrichment of iron atoms provide material source for recrystallization and grain growth of crack healing zone. The existence of micro-voids leads to the hardness of the ferrite in the crack healing zone lower than that in the matrix.

The evolution of internal stresses in the microstructure during quenching is influenced by volume variation and transformation plasticity. Mathematical models were used to prescribe the eutectoid phase transition and some researchers implement the classical nucleation and growth theory to model the microstructure of a given austenite grain size cooling down with different rates to the ferrite- transformation temperature range (Ray, 2011).

During the welding of austenite, the microstructure is refined and converted into bainite so that the strength and impact toughness of the base metal is improved. Heat input rate is the most significant parameter for controlling width of HAZ and with increase in welding speed `width of HAZ. Proper control on welding speed then becomes the important parameter for controlling the HAZ (Ajay N. Boob and Prof. G.K.Gattani)

As the heat input and welding speed both increase, the weld pool becomes more elongated, shifting from elliptical to teardrop shaped. The higher the welding speed, the greater the length–width ratio becomes and the more the geometric center of the pool lags behind the electrode tip. The cooling rate decreases with increasing heat input and preheating (Kou, 1981)].

During welding, the increase in heat input varies per number of beads per layer which also increases the recrystallized area. The hardness of as-deposited weld metal decreased. The average width of columnar grains increased and the yield strength and tensile strength also decreased. The optimum charpy-v impact properties achieved at 2 KJ/mm. grain size increases and the proeutectoid ferrite in the weld metal increases at the cost of acicular ferrite (Evans, 1982)

As per AWS the thermal condition in welding affect metallurgical structure of weldment, mechanical properties, thermal stresses and distortion. The major factors are

(1) The solidification rate of weld metal

(2) The distribution of maximum temperature in weld heat affected zone

(3) The cooling rate in weld metal and HAZ

(4) The distribution of heat in weld metal and HAZ [6].

2.4 MICROSTRUCTURE OF CARBON STEEL

The microstructure of steel is responsible for the macro-behaviour of steel or in other words steel's material properties. Understanding the concepts and phenomena related to microstructure helps to perceive the relation of defects characterization and solid-solid phase transformation with optimum cooling rate of as-cast slabs of specific steel grade (Rana and Dey 2021). These topics, including microstructural phases, the steel classification and cleanliness of the steel, are defined briefly in this section.

It is general knowledge that the material components and their arrangement with respect to each other influence the material properties. Properties of elements and compositions in the microstructure and compositional arrangement in the microstructure define the properties of the unit cell in steel. The long-range arrangement of these units in a crystal

structure determines local and global properties of the crystal built by these unit cells. The complexity of arrangement and variety of microstructure's unit cells are responsible for the difference between the properties of the unit cells and the properties of bulk material (Yan, 2015). These arrangements in the microstructure depend on the history of the material relevant to different phenomena such as previous mechanical and thermodynamic processes on the material. Unit cells with the same arrangement grouped in a single crystal are called grains and borders of this similar arrangement of unit cells, are defined as grain boundaries. Properties of the collection of different crystals in polycrystalline material depend on grains and grain boundaries. These factors specify the steel's property as polycrystalline texture.

Different grades of steel have different material properties because they contain different chemical compositions. However, steels with the same grade experiencing a different heat treatment process or deformation processing have different properties (Kuziak et al., 2008).

Siegel (1978) used a conformal mapping technique to approach the continuous casting (CC) process. In this approach, the ingot interface shape was obtained either for the liquid metal at the solidification temperature or for the solid and the liquid interface by transferring a uniform heat flux to the interface. The complexity of the conformal transformations required in the mapping method made it difficult to treat other types of interface heating conditions. Siegel (2014) approached the CC process by assuming the spatial variation of the heating of the interface by the liquid phase to be a known function. In his two-region model, conduction was assumed to be the only mode of heat transfer. The results were obtained by a Cauchy boundary method. In the present work, laminar code validation was done against results obtained by this method.

Proell (2020) approached phase change problems by using the equivalent heat capacity method. The latent heat of fusion was taken into account by using a linear interpolation of the nodal temperatures. This scheme was independent of solidification interval and, hence, could be used for both pure metals as well as alloys.

Wolf and Viskanta (1988) performed a combined experimental and numerical study of solidification of a pure metal in the presence of liquid superheat. Temperature and position of the interface were used to deduce the importance of natural convection in the liquid pool on the solidification process.

Their results indicated the need of a computational scheme that was capable of simultaneously tracking several moving boundaries (such as solid-liquid, solid-gas and liquid-gas) that occurs when a material shrinks upon solidification. The numerical results in the current work were compared with the experimental results of Wolf and Viskanta (1988). Zabaras et al. (1994) used a front tracking finite element method to calculate the temperature and stress field development in solidifying pure metal. In this approach, interface velocity and location were treated as primary variables and rate dependent viscoplastic-hypoelastic models were employed to determine the stress state on the interface. Their results indicated that the melt pressure significantly alters the deformation at the early stages of solidification.

2.5 Microstructural Phases

Sherby et al., (2008) stated that low iron carbon alloys with carbon content between 0.02% and 2.1% by weight are considered as steel. The microstructure configuration of solid steel is defined by the phases present in the steel microstructure. A defined layout of iron and carbon in steel is recognized as a specific phase in steel. Steel microstructure may be

formed by more than one phase depending on its grade and previous heat treatment. The type, fraction and number of each phase present in a steel microstructure as well as the position of these phases with respect to each other, mainly define the properties of the steel.

Iron carbon phase metallurgy is an arrangement of iron and carbon atoms with respect to each other, which, like the physical definition of a phase, have the same crystallographic structure, density, index of refraction and/or other uniform chemical composition, and physical properties. It is known that we can produce various desired microstructures such as bainite, martensite, cementite (iron carbide, Fe3C), ferrite (α-iron) , pearlite (ferrite, cementite), ferritic-pearlitic, austenite and some other microstructures or different percentages combination of them by controlling cooling rate of hot steel from the austenite temperature (Allazadeh, 2009).

Much work has been done to produce a specific microstructure of steel using suitable cooling techniques. Many different heat treatment techniques and processes are deployed to achieve a microstructure with defined characteristics such as, spheroidizing, full annealing, process annealing, normalizing, quenching, martempering (mar quenching), quench and tempering and austempering, flame hardening, induction hardening, carburizing (e.g. pack carburizing, liquid carburizing, gas carburization) (Banerjee, 2017).

2.6 Solidification of carbon steels

Symeonidis et al.,(2009) stated that solidification can be monitored by thermal analysis (TA), in which the temperature of the metal is recorded over time. From the peak temperature at the left hand side, the molten alloy is cooled down towards the nucleation

temperature of the α-Al dendrites; the curve shows the undercooling needed to form the α-Al dendrites. If grain refiners are added, the required undercooling becomes less, and so the cooling curve can give information about the grain size in the casting.

The next region, between α-Al nucleation and eutectic nucleation, is where the α-Al dendrites grow and fill the casting. Growth after the dendrites have filled the casting will only occur laterally. This region is thus related to the SDAS, which is a common way to evaluate the local solidification time in a casting. Sometimes, especially in high pressure die castings, the SDAS can be hard to distinguish; in this case another measurement, called cell size or cell count, can be used. Cell size or cell count is the number of rounded Al-phase features in a measured length.

The second undercooling is related to the eutectic nucleation, and will give information about the modification level of the Si particles in the eutectic; a smaller undercooling indicates a higher level of modification. The temperature of eutectic nucleation also becomes lower for a modified alloy. The last reaction is related to the precipitation of intermetallics such as, Al2Cu and Al5Mg8Si2Cu2.

Kang and Jaluria (1993) used the enthalpy method, assuming a heat transfer coefficient at the surface of the material to solve I-D two zone and 2-D problems. Their results revealed that the interface shape and the resulting temperature fields were strongly dependent on the withdrawal speed and the cooling rate in the mould. For a small Peclet number, their results were in good agreement with the previously published analytical results.

Amin et al. (2002) referenced Saitoh and Sato (1994) who adopted a boundary-fixing method (BFM) to handle the moving boundary and verified the forced and natural convection effects in the two dimensional CC process. In the BFM technique, they considered the arbitrary geometries of both the moving interface and the domain boundary

via the change of an independent variable, thereby reducing the original problem into the one-dimensional fixed boundary problem. They also analysed the effects of control parameters on uniform and nozzle flow models of CC process. Their results suggested that the location of the solidification front was strongly dependent on the Peclet number.

In spite of these, in production and manufacturing networks where metal mill plates is a critical enabling technology, the quality of welding is highly essential and cannot rely only on quality management systems as mentioned. Even though ISO 9001 has been considered as a stand-alone quality standard, in metal industry, there is the need for more robust quality requirements. Moreover, due to increasing applications of welded products in relation to customer demands as well as health, safety and environmental issues, welded metallic products are therefore required to demonstrate quality attributes such as reliability, efficiency and consumers safety in a wide range of applications. This is evident in applications such as offshore structures where welded metallic products are made to withstand harsh environmental conditions (Royal Dutch Shell Plc., 2011).

Regardless of the product, quality must be efficiently ensured, thus meeting sound quality requirements (Gyasi et al., 2014). However, these attributes of a welded metallic product cannot be built only in the final stages in welding operation since the act and process of welding itself is characterized as a "special process in that the final result may not be able to be verified by testing, thus the quality of the weld is manufactured into the product, not inspected" (Finnish Standard Association -SFS, 2005). For this reason, metallic products require being quality assured through quality control and quality management systems before, during and after manufacturing operations. Most research papers about metallic quality tend to focus on ways of achieving quality with respect to manufacturing processes and parameters, welding techniques, material types, welding consumables or a

combination of either of them, and or monitoring of metallic product quality. However, very few papers have made mention of the needed requirements to achieving quality in metallic products.

Ratnayake presented five "Ps" of metallic manufacturing quality in his paper as suggested by Lincoln Electric Company. It was so that, in order to achieving quality in metallic products, requirement such as: process selection, preparation, procedure, pretesting and personnel must be considered (Ratnayake, 2013). Contributes made by other authors suggest that metallic product quality could be obtained if the design of the joint, electrode, technique, and the skill of the manufacturer are acknowledged (Cary and Helzer, 2005). However, achieving the required quality in a metallic product cannot be fully obtained by following general hypothesis or emulating only quality management system guidelines or standards such as ISO 9000:2005. As manufactured metallic products are bound to compete on both local and international markets, quality must be built in them right from the onset. It is therefore required that companies whose operations chiefly depend on manufacturing of metallic products should comply with international quality standards in order to meet the expected quality in their metallic products.

2.7 Solidification process in steel

The steel used in the experiments of this study were produced by the continuous casting method. Although the purpose of this dissertation is neither the study of steel manufacturing processes nor the formation of microstructure of steel during solidification, it is useful to have a short walk through in the continuous casting steel slab manufacturing process to understand how control of cooling the solidified slab can modify the microstructure of the slab to produce better quality steel. Studying the processes of

continuous casting steel provides the knowledge of the phenomena involved in the formation of the cast slab microstructure and anomalies.

Solidification is a major source of creation of anomalies in the bulk material. In addition, residual and local stresses around anomalies or in the vicinity of grain boundaries are the source of micro crack or crack propagation during heat treatment and cooling of solidified hot steel.

Crack propagation can also be prevented by anomalies formed and distributed during solidification. They provide evidence of the relation of solidification for the behaviour of rate and method of cooling of as-cast hot slab and later operations such as heat treatment and machining (Allazadeh, 2012).

Asai and Szekely (2015) used a stream function vorticity-based method in conjunction with a simplified turbulent model based on a mixing length approach in the coupled fluid and heat transfer in CC steel systems. While this approach enabled tracer dispersion to be calculated, in this regard, the agreement between measurements and predictions was less satisfactory. Ability to estimate the trajectory of inclusion particles within the mould pool was an attractive feature of the model. This method also established that a region of reverse flow is inherently associated with the use of straight nozzles.

Consequently, it is essential to review the solidification process in continuous casting steel production within the scope of this dissertation. The continuous casting method has many advantages such as increase in yield, better surface condition and internal quality of production, more uniform product, higher manpower productivity, easier integration into metal production systems and reducing metal production cost by saving time, energy, and capital. This is due to eliminating extra steps, such as ingot teeming, stripping, and transfers; soaking pits; and primary rolling machining (Allazadeh, 2010).

George Seller (2010), got a patent on continuous casting of metal for producing pipe in 1840. Henry Bessemer patented process for the manufacturing of continuous sheets of iron and steel in 1946. Thereafter, many inventions and modifications helped continuous casting process technology to grow to become the primary technique in producing ferrous and non-ferrous metals. The first vertical type large slab machine with bending of the strand to horizontal discharge was launched in 1961. Detailed historical aspects of continuous casting can be found in many papers.

Today, annually 750 million tons of steel in the steelmaking operation, 20 million tons of aluminium and many tons of other alloys are directly cast from molten metal. In this process, a ladle filled with hot metal is rotated from the electric or basic oxygen furnace to a cast machine on top of the rectangular or delta and "T" shapes bath called a tundish. Molten metal is delivered from the ladle to the tundish after ladle treatment like alloying or degassing via a refractory shroud. Inserting argon gas causes a fully turbulent transient fluid motion in the tundish (Ahmad et al., 2014)). The main function of the tundish is to create a continuous, steady, and stable flow of liquid steel into the mould during draining of the ladle. The mould is tapered to compensate for metal shrinkage on solidification. It provides better heat transfer and, more importantly, fewer cracks.

Xu et al., (2011), introduced the oscillating mould system to the continuous casting. Lubrication and oscillation of the mould decrease the friction to avoid sticking of the solidifying steel, shell tearing, and liquid steel breakouts. Researchers found that the length of stroke and frequency of oscillation affect the quality of the steel and should be specified depending on the type of the steel. The lubricant is the powder added to the molten metal. Sintering and melting of mould powder added to the top of the steel surface protects the liquid flux layer (Sighinolfi, & Paganelli 2011).

The powder flows over the liquid steel due to its low melting point and creates a lubricant between the shell and mold. This enhances the cleanliness of the steel by trapping the inclusions and other impurities and protects the metal from re-oxidation. To emphasize the effect of the mold in steel cleanliness, McPherson used the term “Mould Metallurgy” (Sighinolfi, & Paganelli 2011). However, it has other functions like increasing oxide inclusion separation. The mould provides a solid shell with sufficient strength extended up to the entry of the secondary spray cooling zone.

Radioactive experiments and practical observations show that the meniscus the molten metal starts to lose its superheat and forms the initial shell. Various hypotheses were published to describe the mechanism of first shell formation. Controlling the reciprocation process and heal time by the casting speed put the skin under compression. This causes the confrontation between the pressure of the inner still liquid metal and contraction of the mould near the skin, which gives an odd shape to the solidification profile other than a simple square shape (Saitoh, and Sato, 2014). The nozzle clogging can create fluctuation level in the mould and can be reduced by improving the cleanliness of the steel and the Ca treatment at the ladle furnace. A number of experiments and theoretical models have been used to study steel solidification from the moment it leaves the tundish to the time it is quenched after it has cooled in the mould (Saitoh, and Sato, 2014).

Other researchers target other areas in the steel making processes to lower the final cost of the steel. All these procedures are very complex and precise and a miscalculation can damage the machines or stop production, which increases cost. Cracks and other anomalies are created during the solidification process. Dissipation of superheat and temperature at the meniscus entrap the inclusion and gas bubbles, and turbulent flow and liquid-liquid

and liquid-solid phases‟ interactions. Furthermore, thermal and solute buoyancies effect of surface tension take place during solidification of steel (Saitoh, and Sato, 2014).

Steel production in the vertical bending (VB-type) caster contains a lower amount of inclusions distributed deeper compared to the curved caster (S type). The driven force to move the strand forward is provided mainly by the rollers. However, gravity has an effect on the speed of the strand in vertical casting. Applied forces during the solidification process affect the quality and soundness of steel. Some of these forces are external and residual stress generation, tension, oscillation and gravity-induced waves, residual distortion and wear along the mould, microscopic and macroscopic coupled with segregation (Thomas, Najjar, and Mika, 2010).

At secondary cooling molten steel is encapsulated by a solidified skin and water spray which causes the release of superheat from the inner section of the steel. However, poor thermal 1819 conductivity of steel limits the effectiveness of spray cooling and, in return, results in reheating the surface (Yeh, and Chung, 2015). The quality of the secondary cooling process was the subject of many investigations (Yeh, and Chung, 2015). Higher cooling rate increases exogenous inclusions by increasing the possibility of entrapment (Yeh, and Chung, 2015).

Different methods such as dynamic control of continuous casters and dynamic spray cooling model are used to control the temperature of the strand in continuous casting. Thermal tracking of the slab cooling history is accomplished by dynamic control of continuous casters suggested in the literature (Yeh, and Chung, 2015). Dynamic spray cooling includes techniques such as control points along the caster length, through slab slices, combined feedback with feed-forward and curve fitting (Allazadeh, 2015)

During the secondary stage, liquid steel is solidified to semis. Three important factors determine the type of the microstructure develops during the solidification of a casting. These factors are;

- The temperature gradient in the liquid ahead of the liquid–solid interface (G);
- The velocity of the liquid–solid interface (V)
- The alloy composition (C0).

Depending on the G/V ratio, the microstructure is planar at first to cellular and then to dendritic, as G/V gets smaller. Hence, usually three zones in the macrostructure of a continuously cast steel semi can be recognized. These zones from the surface towards the centre are chilled crystal zone, columnar zone and equiaxed zone, respectively (Zhong, 2021).

2.8 Parameters in the quenching processes

Parameters affecting the cooling rate include: quenchant type, quenchant temperature, agitation velocity, viscosity, agitation type, aging, polymer foaming, polymer degradation, part material, geometry, part area, part volume, density, specific heat, oxide layer, surface roughness, suspension, carbon content, grain nature, grain size, plastic deformation and number of other issues (Dossett and Totten, 2014). Therefore, to perceive the goals of the experiments in this research work, it is important to review the previous work on three main subjects involving the determination of optimum cooling rate of steel from the critical temperature ranges. These experimental topics are quenching, phase transformation and crack formation in steel subjected to thermal gradients.

The subject of optimum cooling rate is mainly related to the quenching, which consequently, helps to establish the desired cooling rate through the material. Quenching is accelerating cooling with a quenchant such as air, water, oil, salt, natural or vegetable base quenchant, polymers and other chemical compounds (Pedišić et al.2014).. Liquid quenching is more common in industry because it furnishes a quenching process with homogeneous and more controllable heat transfer from the hot body.

Three stages of quenching for a liquid quenchant are: vapour stage, boiling stage and convection stage (Ramesh and Narayan 2014). Time-Temperature-Transformation diagrams (TTT) for any grade of steel is the outcome of controlled cooling rate using the cooling agents.

However, there are two problems with these controlled cooling methods. First, any participation may vary the shape of the TTT diagram and, secondly, as the cooling rate increases, the residual stresses stored in the bulk material increases as well (Beretta & Murakami 2018). The first factor makes the final product case dependent on the steel grade with different chemical composition and the second one may result in higher defect density in the microstructure. The other problem is that the TTT curve may not maintain its shape in the presence of different levels of residual stresses. These facts make the prediction of quenching complicated. There are many publications on the quenching topic, which provides the information about different quenchants and the thermodynamic and chemical properties (Ramesh and Narayan 2014).

In a more general definition, quenching is a metallurgical process for controlled extraction of heat from material depending on the interfacial chemical properties of the material quenched (Ramesh and Narayan 2014). Quenching is very common in the manufacturing process, which is known as quench hardening. Factors, which are considered in quenching

hardening, are residual stresses and distortion, prevention of crack initiation, microstructural evolution necessary to improve properties (wear resistance and toughness), and meeting the desirable hardness (Ramesh and Narayan 2014).

Application of quenching in steel manufacturing is done to obtain the desired mechanical properties such as, hardness, yield strength, and ductility (Dewangan et al.2020). The material properties are controlled by a quenching process in many industrial applications, e.g., in engine components for wear and durability, aircraft components for strength and fracture toughness, bicycle frames for strength, lightness and durability (Dewangan et al.2020).

Parameters, which shall be considered in the quenching process of a bulk material, are desired suspension, cooling rate, cooling nature, heat transfer coefficient, residual stress, desired hardness and other material properties, distortion tendency, and cracking potential (Dewangan et al.2020). For liquid quenchants, heat transfer rate is the most important factor in controlling the heat transfer rate and it decreases exponentially with increasing viscosity. Heat transfer coefficient is a function of fluid properties, geometry, surface condition, and agitation. Heat transfer depends on heat transfer coefficient, time and location within the bulk material. Rewetting process and agitating as well as the variation of chemistry of the quenchant during the cooling process must be monitored and controlled in designing an optimum cooling rate (Albano, 2012)

Cooling steel from the austenite temperature may result in different transformation sequences and the allotriomorphic phase proportions such as ferrite, pearlite, Widmanstatten ferrite, bainite and martensite. The discussion on solid-solid phase transformation has been the subject of many conferences around the world (Sarkar et al., 2021). Many of these studies were devoted to predict the microstructure at room

temperature resulting from these transformations. A large body of literature exists in which the subject of solid-solid transformation has been discussed from different aspects. Sarkar et al., (2021) discussed the critical points of phase transformation in solids. Soffa and Laughlin (2011), discussed diffusional instabilities by examining data from observations, X-ray, electron diffraction, transmission electron microscopy (TEM) and atom probe field ion microscopy (APFIM).

Study on precipitation of pro-eutectoid phases in the literature gives the microstructural analysis for different temperature and positions of samples (Hoedle, Frauenhuber, & Moerwald, 2009). Two main transformations determined the phases formed from austenite. These mechanisms are reconstructive transformation and displacive transformation. Reconstructive transformation is a slow rate process controlled by diffusion. The main resulting phases of this transformation are ferrite and pearlite. It occurs in the high temperature regime by movement of atoms at the transformation interface. Bhadeshia (2011) has suggested some modes to decrease the temperature of solid-solid phase transformations. Driven force for polymorphic austenite to ferrite transformation is greater than grain growth by two orders. Therefore, non-metallic inclusions get involved in the decomposition of austenite rather by original austenite grain size and concentration than mobility of the boundary. Displacive transformation is a rapid process without any movement of atoms across the transformation interface. This transformation occurs rather via deforming shape of an invariant plan strain by a large shear component. Austenite phase mainly transforms to Widmanstatten ferrite, bainite and martensite (Bhadeshia, 2011).

In transformation, austenite with an FCC crystal unit cell with slow cooling rate is transformed to the BCC ferrite unit cell. Martensite is a diffusionless process and carbon is left in solid solution, which results in transforming FCC austenite to BCC or BCT lattice under high cooling rate processes (Bhadeshia, 2011). Speich and Miller (2014) stated that the amount of martensite in the final microstructure depends not only on carbon content but intercritical phase transformation temperature and given cooling rate.

Ge et al. (2018) studied tempered martensite microstructures and found a relationship between their chemical composition and thermal history with their mechanical properties. Calcagnotto et al. (2011) performed tensile tests in quenched samples and concluded that in the presence of a stress field the martensitic point and the plastic behaviour of material not only change the temperature but change in the temperature. Research on the composite materials with fiber or particles embedded in the body led to predict fracture formation due to inhomogeneity of material, as well.

Ge et al. (2018) experimental results showed that the tendency for crack formation is higher with a range of cooling rates and it decreases for the cooling rate higher or lower than this critical cooling rate range as a function of quenching rate. The factors governing the behaviour of material at high temperature are time, temperature, stress, and environment or atmosphere. At low temperature mechanical behaviour like fatigue damage, is controlled by the level of the mean stress, amplitude of stress fluctuation and number of cycles (Kobasko, 2010).

Quasi-cleavage may occur within regions of grains with different orientation in quenched and tempered steels, and they may result in lower resolved normal stress and, consequently, ductile fracture mode (Ge et al. (2018). Three major fracture modes in the microstructure are ductile fracture by nucleation and growth of voids, and brittle fracture

via trans-granular fracture or inter-granular separation. The transgranular cleavage is the most common one. In ferrite, it adopts both Griffith (energy) and Orowon (stress) criteria and, according to the Hall Petch equation, grain refinement requires higher debounding fracture stresses (Calcagnotto et al. 2011). Calcagnotto et al. (2011) analysed the length of longitudinal cracks on the surface of continuously cast steel slabs and gave crack frequency as a function of crack length using fractal distribution methods. Quantitative characteristics of the crack growth are peak load of the force displacement curve, nominal specific energy of the formation of new unit surface, average force, and fractal dimension of fracture surface and height of the surface roughness peaks (Calcagnotto et al., 2011). Cracks initiate or propagate in a different manner depending on the microstructure, composition and properties. Tensile test experiments on tool steel showed that cracks initiate (or exist) in the carbide band growth straight forward in the matrix and after kink type dislocation in the carbide rich region split in the same direction of the region then jump to the next carbide band and grow in the same manner and so on.

Computer simulations have been deployed in the last decade to lower the cost of microstructural experiments. Much work on modelling of thermo-mechanical treatments of steel has provided the capability to predict the final microstructure (Ge et al. (2018).

CHAPTER THREE

MATERIALS AND METHODS

3.1 Introduction

This chapter looked at the materials, equipment and methods used. That is, the composition of the base metal, specimen size and thickness. The type of electrode used and its composition, the edge preparation as well as the testing machine used and the type of testing carried out. The low carbon steel plates of thicknesses 12mm scrap and 12mm new and were used which is normally used by most people in the construction industry in Ghana. The samples were prepared according to the mechanical testing parameters (i.e. tensile test, impact/compressive test and hardness). The chemical analysis was done on the specimen and recorded in table 1

The preparation of specimen and welding was done at the Tema Steel Works Company and the Kwame Nkrumah University of Science and Technology welding workshop. The welded metals were taken through heat treatment processes, that is Normalizing and Hardening using air, water and oil.

Standard mechanical tests was done using both new and scrap carbon steel plates. Accordingly, the following machines and equipment were used for the study; standard tensile test machine (for tensile testing), impact test machine (for impact/compressive), an electric Arc welding machine, an angle grinder for cutting the specimens and electrodes for the welding process all carried out at the Kwame Nkrumah University of Science and Technology welding workshop, Ghana.

3.2 Materials

The sample of specimen used was 215mm long x 35mm width x 12mm thick scrap and new carbon steel plates.

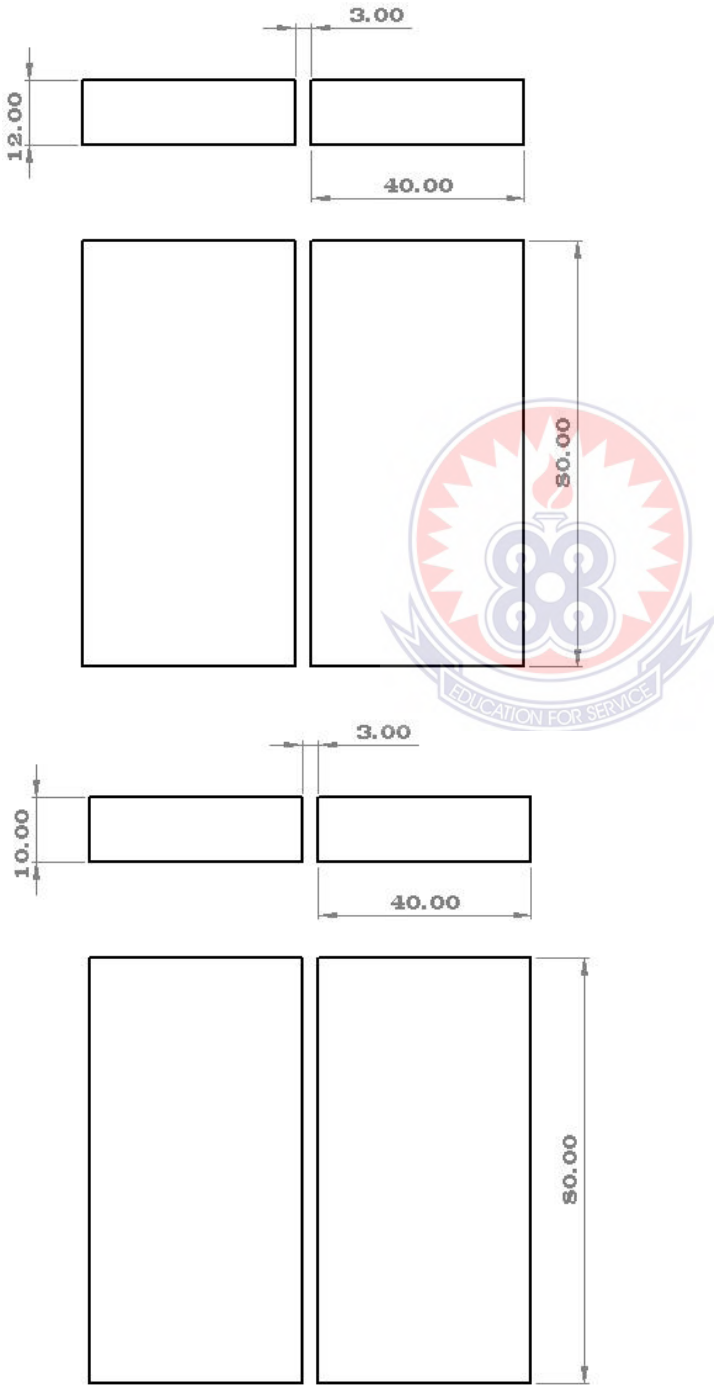

Figure 3.1 A dimensional sketch of weld joint

3.2.1 Chemical Composition of Specimen

The Chemical composition of the base metal was analysed as shown in table-1. The composition consist of the following; Carbon, Silicon, Manganese, Phosphorus, Sulphur, Chromium, Nickel, Vanadium, Titanium, Aluminium, Copper, Cobalt, iron, and Molybdenum.

Table 3.1 Chemical Analysis of Materials Used

Sample No	C %	Si %	Mn %	P %	S %	Cr %	Ni %	V %	Ti %	Al %	Cu %	Co %	Fe %	Mo %
Metal 12mm scrap	0.115	0.126	0.653	0.014	0.024	0.001	0.145	0.018	0.013	0.001	0.042	0.363	96.18	0.054
Weldment	0.168	0.241	0.274	0.044	0.026	0.001	0.0221	0.028	0.017	0.001	0.138	0.298	96.19	0.048
Metal 12mm new	0.164	0.038	0.323	0.033	0.044	0.001	0.132	0.021	0.013	0.003	0.055	0.274	96.74	0.043
Weldment	0.087	0.225	0.21	0.038	0.033	0.249	0.213	0.011	0.002	0.001	0.147	0.291	96.19	0.057

3.2.2 Preparation of Specimen

The Single V edge preparation with 60° included angle was made on the specimen as shown in Fig. 1.

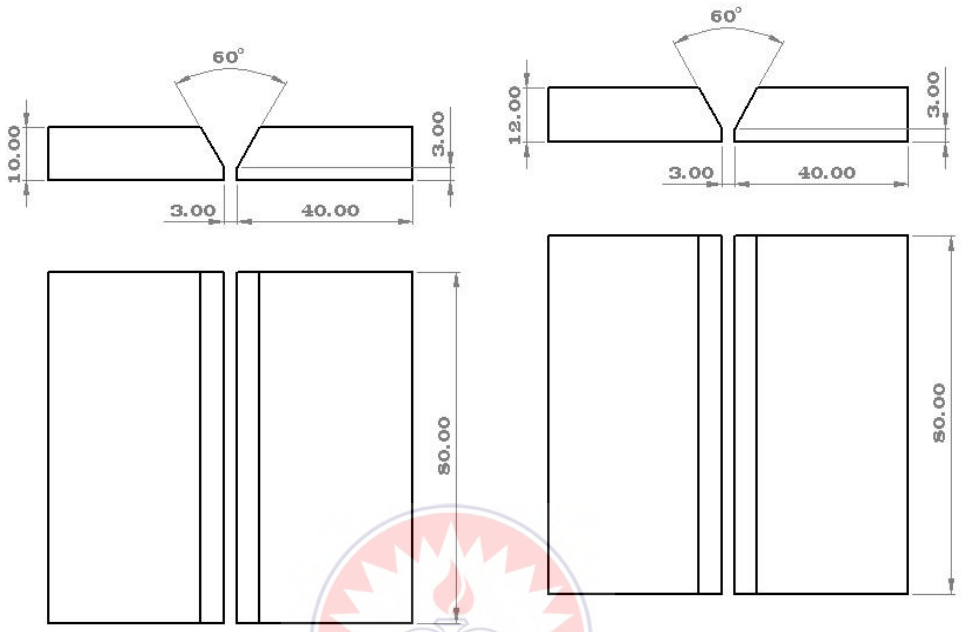

Figure 3.2 Experimental setup

The set-up was made by tack welding as shown in Fig. 2. Root gap and root face was kept at 3mm each. Welding of the different specimens was performed using 1G welding position as shown in Fig 3. Flux coated electrodes that was used for welding was AWS/SFA 5.1 E-6013 of 3.15mm diameter and 350mm long. Chemical composition of electrode that was used is also shown in Table 2. The Welding current of 80, 90, 100 amps was used by keeping the welding speed at 1.52 mm/sec and arc voltage 21 volts constant. Technical specification of welding power source that was used as stated in Table 4 and photograph of welding power source that was used is shown in Fig-7. Welding polarity was kept at DCEP.

The welded specimen was cooled in normal air, water and oil shown in Fig 4-6. Welding voltage was kept at 21, 23, 25 volts and kept welding current at 90 amp whiles the speed

of travel was kept at 1.52 mm/sec constant. Welding polarity was DCEP. After welding, the weld reinforcement was ground and weld joint face made flat.

Figure 3.3 Set-up of tacked weld

Figure 3.4 Welding Position and Process (KNUST Workshop, 2020)

Figure 3.5 Water Cooled Specimen, Scrap and New (KNUST Workshop, 2020)

Figure 3.6 Water Cooled Specimen, Scrap and New(KNUST Workshop, 2020)

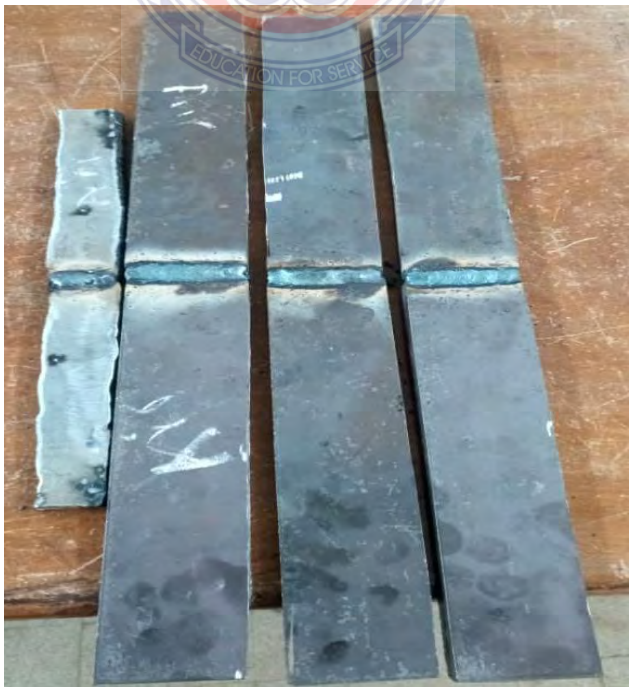

Figure 3.7 Air Cooled Specimen, Scrap and New (KNUST Workshop, 2020)

Table 3.2 Chemical Composition of the E – 6013 Electrode

Element	Carbon	Manganese	Silicon	Sulphur	Phosphorus
Percent %	0.07	0.44	0.22	0.02	0.02

Table 3.3 Technical Specification of the Welding Machine

Model	**DC2013 – T**
Maximum Output Current	300 Amps DC
Output Voltage Power	6 VDC
Maximum Output Power	18 KW
Full Output Duty Cycle	3% @ 3000 A(2% @ 4000 A option)
Control Modes	Current / Voltage / Power
Output Accuracy of Setting	± 1%
Ripple	< 1%
Program Timing Values Squeeze Time	0.1 – 999.9 ms
Upslope Time Pulse 1	0. 1 – 999.9 ms
Peak time Pulse 1	0.1 – 999.9 ms
Downslope Time Pulse 1	0.1 – 999.9 ms
Delay time Between Pulses	0.1 – 999.9 ms
Upslope Time Pulse 2	0.1 – 999.9 ms
Peak time Pulse 2	0.1 – 999.9 ms
Downslope Time Pulse 2	0.1 – 999.9 ms
Hold Time	0.1 – 999.9 ms

Process Monitor Limits	Current / Voltage (Displacement)
Number of waveforms averaged	User defined
Waveform Window limiting range	0 – 100%
Waveform window tolerances	0 – 100%
Optional Feedback Monitoring	Up to 6 channels of real time weld displacement monitoring
Displacement monitoring	LVDT or Encoder
Force Range	0. 500 N (0- 112 lb)
Input Requirements	3 phase
Input Voltage	380 – 480 VAC
Control I/0	Opto isolated
Serial Communications	Ethernet via TCP / IP, USB 2.0, RS232

Table 3.4 Weight & Dimensions of the welding Machine

Dimensions (L x W x H)	**19.6 in x 8.7 in x17.5 in (497 mm x 220 mm x 445 mm**
Weight	84 lb (38 kg)

Figure 3.8 Welding Machine (KNUST Workshop, 2020)

3.3 Mechanical Properties

3.3.1 Ultimate Tensile Strength (UTS)

The Ultimate Tensile Strength of a material is the maximum tensile stress that the material can withstand without failing. In brittle materials, the ultimate tensile strength is close to the yield point whereas in ductile materials the ultimate tensile strength can be higher. The ultimate tensile strength is usually found by performing a tensile test and recording the stress and strain produced. The highest point on the stress – strain curve is the ultimate tensile strength. It is measured in Pascal or N/m^2.

Each of the tensile test specimen was placed in the computerized universal testing machine, with an extensometer connected to it. One end of the specimen was secured firmly to the non-movable jaw while the other end was secured in the movable jaw of the universal tensile testing machine with the specimen at room temperature. The load control

knob (actuator) was subsequently activated to apply a steady tensile load to each of the specimen until the specimen failed.

With the aid of the load sensor attached to the test specimen, the increasing tensile stresses were measured digitally. The extensometer recorded the corresponding changes in the length of the test specimen arising from the application of the tensile loads. The computer monitor connected to the testing machine, digitally generated and displayed a stress-strain graph for each pair of the test specimens. The strain and yield Strength were also obtained using the same machine.

3.3.2 Strain

The Strain of material is the elongation or the increase in length of the material when subjected to tensile stress. It is a description of deformation in terms of the relative displacement of particles in the body that excludes rigid – body motions. Deformations which are recovered after the stress has been removed are called elastic deformations. The deformations which cannot be reversed or returned to its original state is known as plastic deformation.

3.3.3 Yield Strength

The Yield Strength is the maximum stress that the material can withstand before permanent deformation occurs. The yield point is the point on the stress – strain curve that indicates the limit of elastic behaviour and the beginning of plastic behaviour. The yield strength is often used to determine the maximum allowable load in a mechanical component, since it represents the upper limit to which forces that can be applied without producing permanent deformation. It is measured in Pascal or N/m^2.

3.3.4 Elastic Young's Modulus

This is a measure of a material, and it defines the relationship between stress (force per unit area) and strain (proportional deformation) in a material. The slope of a stress strain curve represents the elastic modulus of the material. The relationship between stress and strain is described by Hooke's law which states that stress is proportional to strain, provided the elastic limit of the material is not exceeded. The coefficient of proportionality is Young's modulus. The higher the modulus, the more stress needed to create the same amount of strain. The Young's modulus is calculated using the formula;

Change in length, $\delta = Ln - Lo$ …….

(3.1)

The strain (ε) or relative deformation is the Change in length divided by the original length

$$\varepsilon = \frac{\delta}{Lo}$$ …….

(3.2)

$$\text{Young's modulus} = \frac{\text{stress}}{\text{Strain}}$$ …….

(3.3)

$$E = \frac{\sigma}{\varepsilon}$$ …….

(3.4)

The Young's modulus of carbon steel is around 190 GPa and 215 GPa, the test will help determine the Young's modulus of both the new and scrap carbon steel after welding and heat treated.

Figure 3.9 Computerized Universal Tensile Test Machine (KNUST Workshop, 2020)

Figure 3.10 Specimen in Tensile Machine (KNUST Workshop, 2020)

3.3.5 Hardness Test

Hardness is the resistance to indentation, and it is determined by measuring the permanent depth of the indentation. This research is looking at the effect of the cooling rate on the new carbon steel welded plate as well as the scrap carbon steel welded plate and all the specimens will be tested on Rockwell hardness testing machine. The hardness will be measured at three points i.e. at base metal (before and after welding at 10mm distance from weld center line), HAZ at near to fusion boundary and weld metal center line and will be shown in fig-8. The readings will be noted in observation table-5,6 & 7. Technical specification of Rockwell hardness tester used will be as per table-4. The Rockwell hardness test is the most commonly used hardness test method. It also presents a more accurate result than other testing methods, and can be used on all metals.

Figure 3.11 The Rockwell hardness Testing machine (KNUST Workshop, 2020)

Table 3.4 Technical specification of Rockwell hardness tester

Model	**JG – 101**
Measuring range	20 – 88HRa, 20 – 100HRB, 20 – 70HRC
Initial test force	10Kgf (98.07N)
Total Test force	60Kgf (558.4N), 100kgf (980.7N), 150kgf (1471N)
Hardness value reading	Dial gauge
Carriage control	Manual loading / unloading
Max. height of test piece	210mm
Depth of throat	160mm
Min. Scale value	0.5HR
Dimension	510 x 220 x 700 (mm)
Package dimension	620 x 490 x 780 (mm)
Weight	85 / 100kg

3.3.6 Impact Testing

Impact Testing of metals is usually carried out to determine the impact resistance or toughness of materials by calculating the amount of energy absorbed during the fracture. The impact test is performed at various temperatures to uncover any effects on the impact energy.

This impact test was carried out using the HSM55 PENDULUM digital impact testing machine (300J). The of water, air and oil cooled specimen were prepared as shown in Fig. 11, and then welded, cooled in water, air and oil and placed in the tensile testing machine as shown in Fig. 12, the impact is made using the pendulum raised to the require angle.

When the pendulum hits the specimen, it absorbs some energy from the impact of the pendulum and fails as shown in Fig. 13 depending on its toughness and the energy absorbed is referred to as the impact energy which is recorded on the digital display.

The impact strength can be calculated by

$$\text{Strength(S)} = \frac{\text{Impact Energy(J)}}{\text{Cross Sectional Area(CSA)}} \quad \ldots\ldots\ldots\ldots\ldots\ldots\ldots\ldots\ldots\ldots\ldots\ldots\ldots\ldots\ldots \quad (3.5)$$

Figure 3.12 HSM55 Pendulum digital impact testing machine (300J) (KNUST Workshop, 2020)

Figure 3.13 Samples of both scrap and new specimen prepared for impact Test

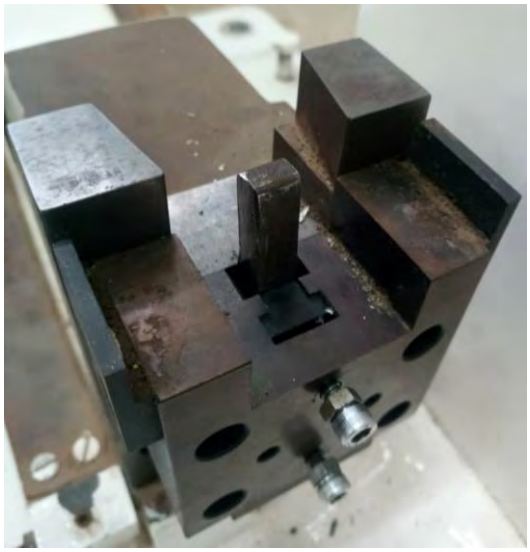

Figure 3.14 Specimen in Impact testing machine

Figure 3.15 Failure after impact Test

CHAPTER FOUR

RESULTS AND DISCUSSION

4.1 Introduction

This chapter presents the results and discussions of the study. There are three types of tests that was conducted in this research, these are the Tensile, the Impact and the Hardness tests which were all conducted based on the ASTM. All the test consists of scrap and new carbon steel plate of thickness 12mm. This section will discuss the results of these tests and evaluate the effects of cooling rate on new and scrap carbon steel metals on welded joints.

The experimental Data obtained was analysed by graphs, tables and charts. The computer-interfaced microscope which was attached to the testing machine generated, plot and displayed the stress-strain graphs for the various sets of sample specimens automatically in the hardness tests and the MATLAB was used to analyse and plot the graphs of the mechanical, tensile, compressive and impact tests where the sets of results for both new carbon steel and scrap metal specimen were compared to determine the effect that the solidification rate has on the welded carbon steel components.

4.2 Hardness test result

4.2.1 Hardness Results Discussion of 12mm specimen

Vickers Hardness test is carried out to obtain the hardness of the specimen. The pyramid diamond indenter is pushed at 30 points for an interval of 2mm as shown in Fig. 15 at the parent metal and 1.6mm at the heat affected zone for each of the specimen type.

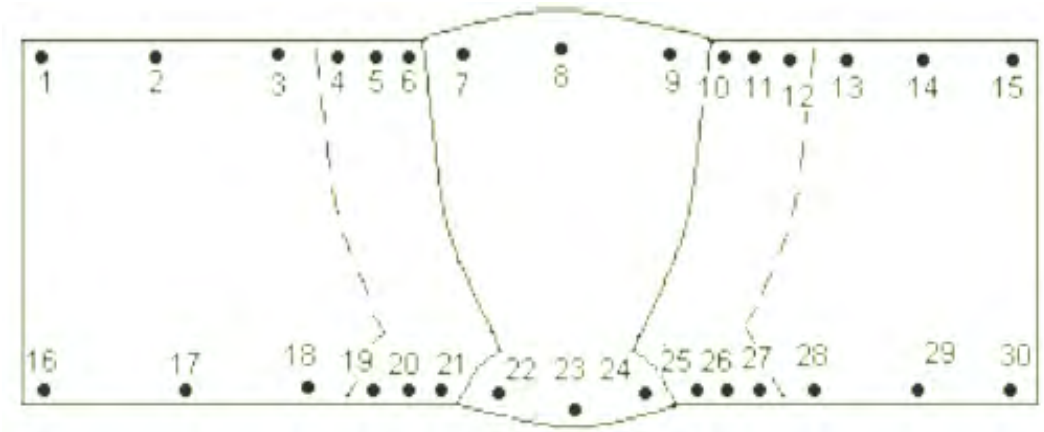

Figure 4. 1 The Welded specimen and the 30 points

4.2.2 Hardness Results Discussion of Water Cooled specimen, 12mm Scrap and New

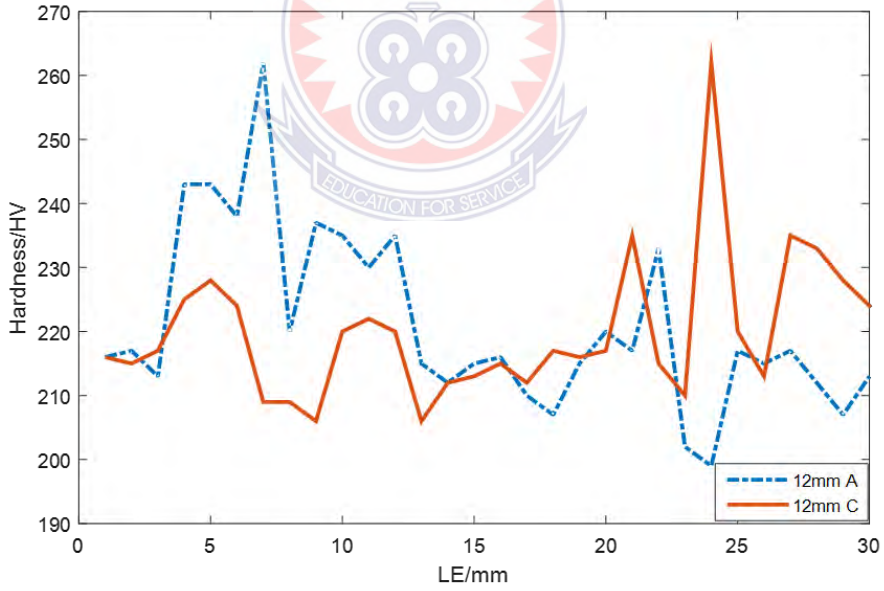

Figure 4. 2 Vickers Hardness Test HV for Water cooled specimen 12mm new and 12mm scrap

A = 12mm New

C= 12mm scrap

From Fig. 4.2, the average Vickers Hardness for the 12mm new is 221.03 HV and the average for 12mm scrap is 219.8 HV. At the weld zone the average hardness is 225.5 HV for the 12mm new and 229.33 HV at the heat affected zone. With the 12mm scrap, the average hardness at the welded zone and the heat affected zone are 218.50 HV and 224.17 HV respectively. From the average HV values of the test results considering the parent metal, welded zone and the heat affected zone, it is clear that the 12mm new water cooled specimen is harder than the 12mm scrap water cooled specimen.

4.2.3 Hardness Results Discussion for Air Cooled, 12mm new and 12mm scrap

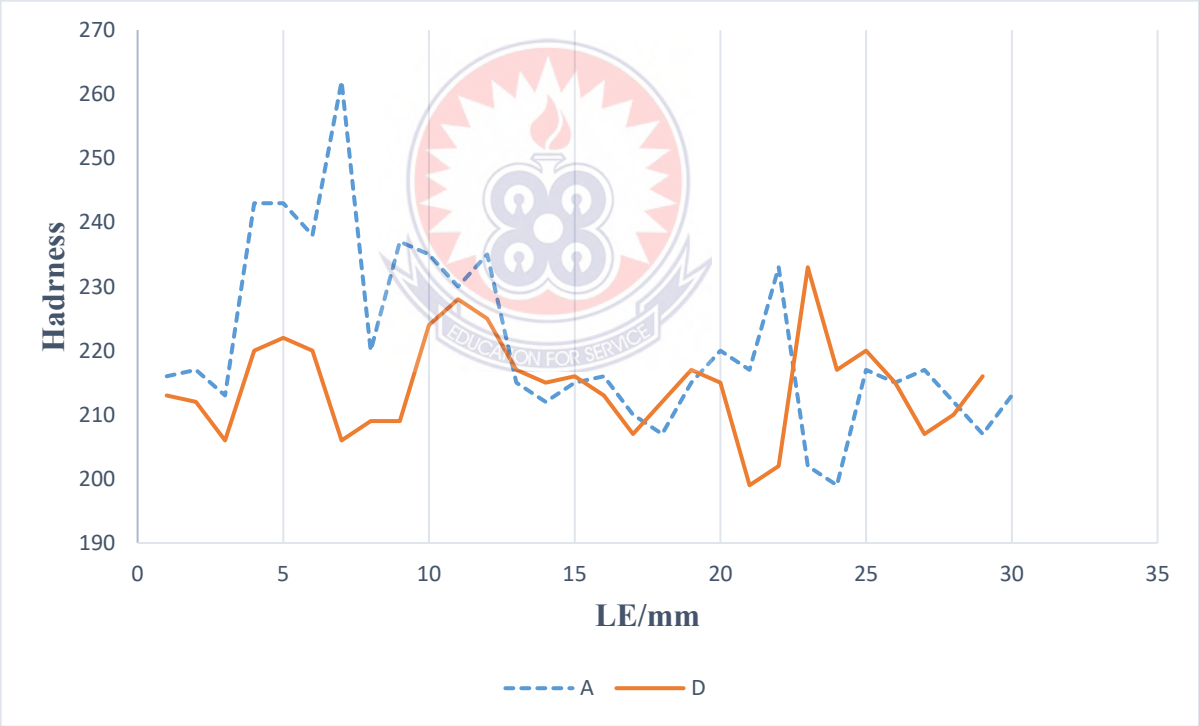

Figure 4. 3 Vickers Hardness Test HV for Air Cooled specimen 12mm new and 12mm scrap

B = 12mm New

D= 12mm scrap

From Fig 4.3, it can be seen that, the average Vickers Hardness for 12mm new is 201.6 HV and the average for 12mm scrap is 214.67 HV. At the weld zone the average hardness is 225.17 HV for the 12mm new and 190.00 HV at the heat affected zone. With the 12mm scrap, the average hardness at the welded zone and the heat affected zone are 212.67 HV and 157.50 HV respectively. From this observation the 12mm scrap air cooled is harder than the 12mm new air cooled

4.2.4 Hardness Results Discussion for Oil Cooled, 12mm new and 12mm scrap4

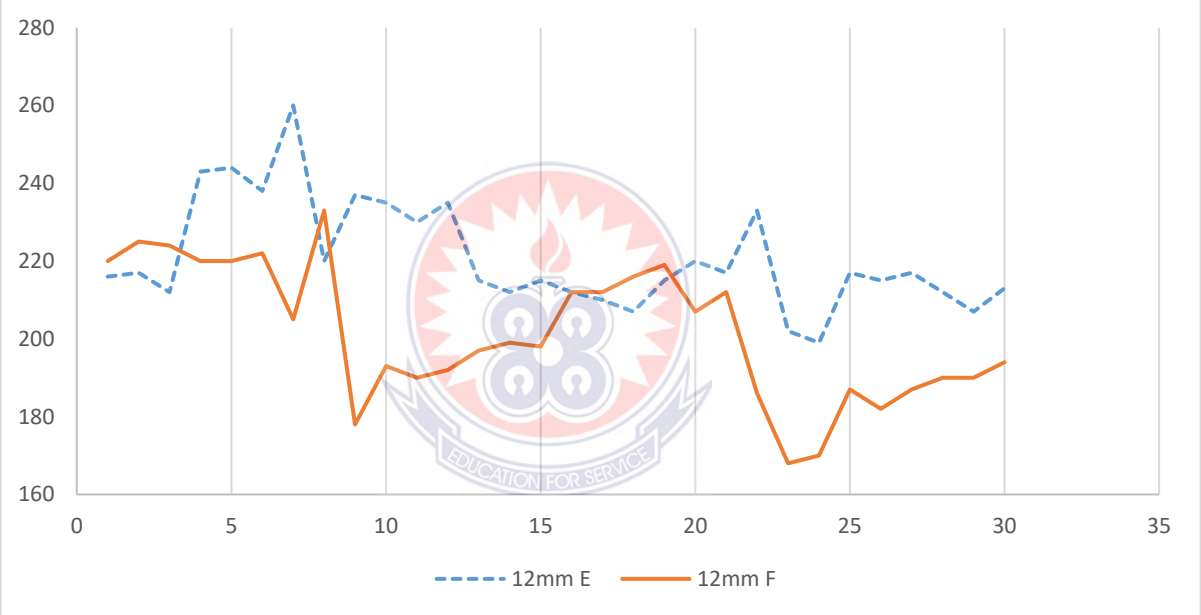

Figure 4. 4 Vickers Hardness Test HV for Oil Cooled specimen 12mm new and 12mm scrap
E = 12mm New

F= 12mm scrap

From Fig 4.4, it can be seen that, the average Vickers Hardness for 12mm new is 220.83 HV and the average for 12mm scrap is 201.60 HV. At the weld zone the average hardness is 225.17 HV for the 12mm new and 229.50 HV at the heat affected zone. With the 12mm scrap, the average hardness at the welded zone and the heat affected zone are 190.00 HV

and 216.67 HV respectively. From this observation, the 12mm new oil cooled is harder than the 12mm scrap oil cooled.

Table 4. 1 Average Hardness Values at Weld Zone for water, air and oil cooled specimen

	New(HV)	**Scrap(HV)**
Water Cooled	239.7	208.0
Air Cool	239.7	208.0
Oil cooled	239.0	205.3

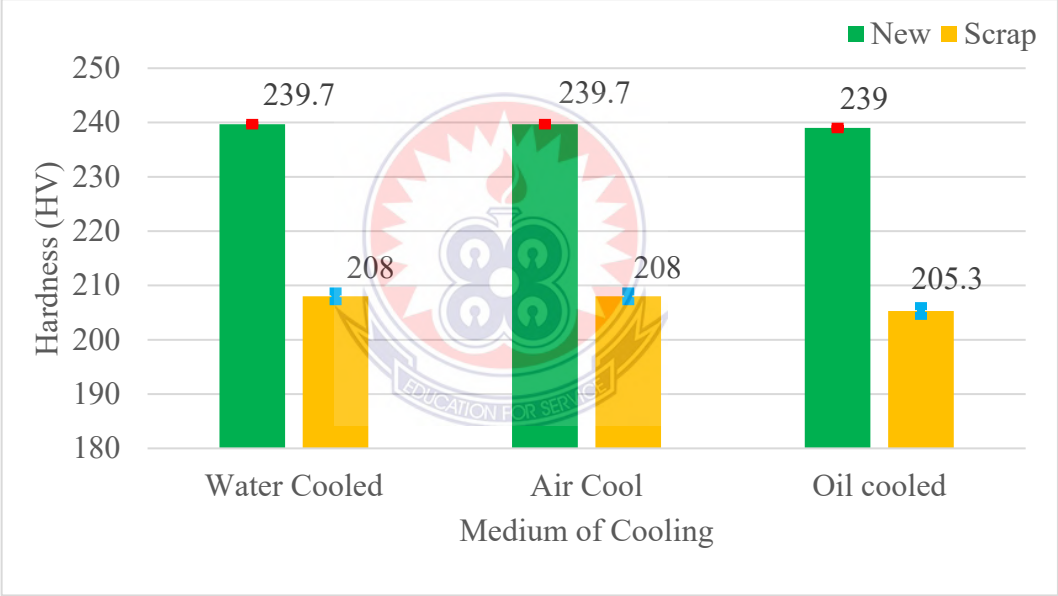

Figure 4. 5 Average Hardness Values at Weld Zone

Fig. 4.5 clearly shows that the 12mm new water cooled specimen is harder than the 12mm scrap water cooled specimen. In the same way, it is also observed that the 12mm new air cooled is harder than the 12mm scrap air cooled. Again, it was realised that the 12mm new oil cooled is harder than the 12mm scrap oil cooled all at the welded zone. This shows that there is a higher effect of cooling rate on scrap carbon steel as compared with new carbon

steel and this confirms the findings of Xin (2017) on the Effect of heat treatment on microstructure and hardness of internal crack healing in a low carbon steel.

4.3. TENSILE TEST

With this analysis, the properties that are directly measured by a tensile test are ultimate tensile strength, strain, yield strength and Young's modulus. This tensile test was carried out using the PROETL: DI-CP/V2 2000KN. The test was carried out on the welded specimen after heat treatment (Normalizing and Hardening). The cooling was done by water, air and oil for three samples for both scrap and new and the results shown in Figs. 19 to 22. The tensile test machine generated the stress strain graph for each test. The data was extracted using MATLAB and the results of water, air and oil cooled re-plotted on the same graph for comparison and analysis purposes.

4.3.1.1 Tensile Test Results for 12mm New Specimen (Water, Air and Oil Cooled)

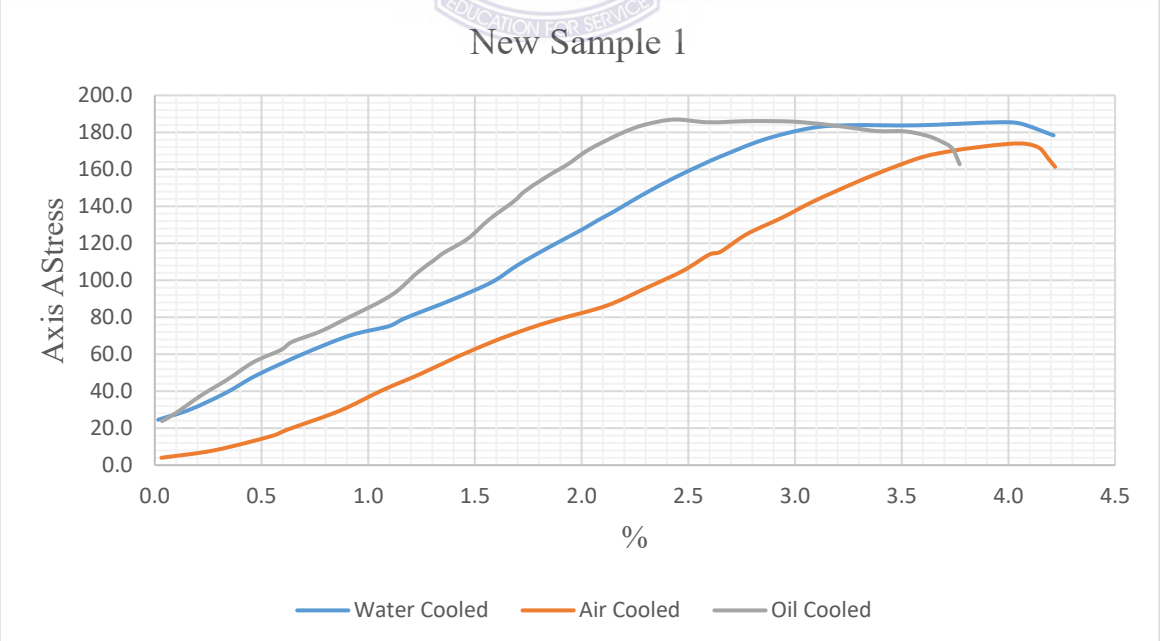

Figure 4. 6 Stress Strain Test for 12mm New Specimen (Water, Air and Oil Cooled)

Air Cooled

The Thickness for the specimen was 12, its width was 63.5, with an Area of 726.0mm^2 and Gauge length of 300, all dimensions are in mm. The Tensile test produced the following outcomes.

Table 4. 2 Outcome of Tensile Test

Description	Value	Unit
Force max	189.384	kN
Tensile stress Su/Rm	248.8	N/mm^2
Yield stress YS/Rt(.5%)	68.1	N/mm^2
t%	0.5	%
Total elongation EI/ (A)	2.6	%
Young modulus E	13.44	kN/mm^2

Oil Cooled

The Thickness for the specimen was 12, its width was 63.50, with an Area of 762mm^2 and Gauge length of 300. All dimensions are in mm. The Tensile test produced the following outcomes.

Table 4. 3 Outcome of Tensile Test

Description	Value	Unit
Force max	185.592	kN
Tensile stress Su/Rm	243.6	N/mm^2
Yield stress YS/Rt(.5%)	80.5	N/mm^2
t%	0.5	%
Total elongation EI/ (A)	1.7	%
Young modulus E	13.92	kN/mm^2

Water Cooled

The Thickness for the specimen was 12, its width was 63.50, with an Area of 762mm^2 and Gauge length of 300. All dimensions are in mm. The Tensile test produced the following outcomes.

Table 4. 4 Outcome of Tensile Test

Description	Value	Unit
Force max	186.549	kN
Tensile stress Su/Rm	244.8	N/mm^2
Yield stress YS/Rt(.5%)	83.7	N/mm^2
t%	0.5	%
Total elongation EI/ (A)	1.4	%
Young modulus E	11.72	kN/mm^2

4.3.1.2 Tensile Test Results for Sample 2, 12mm New Specimen

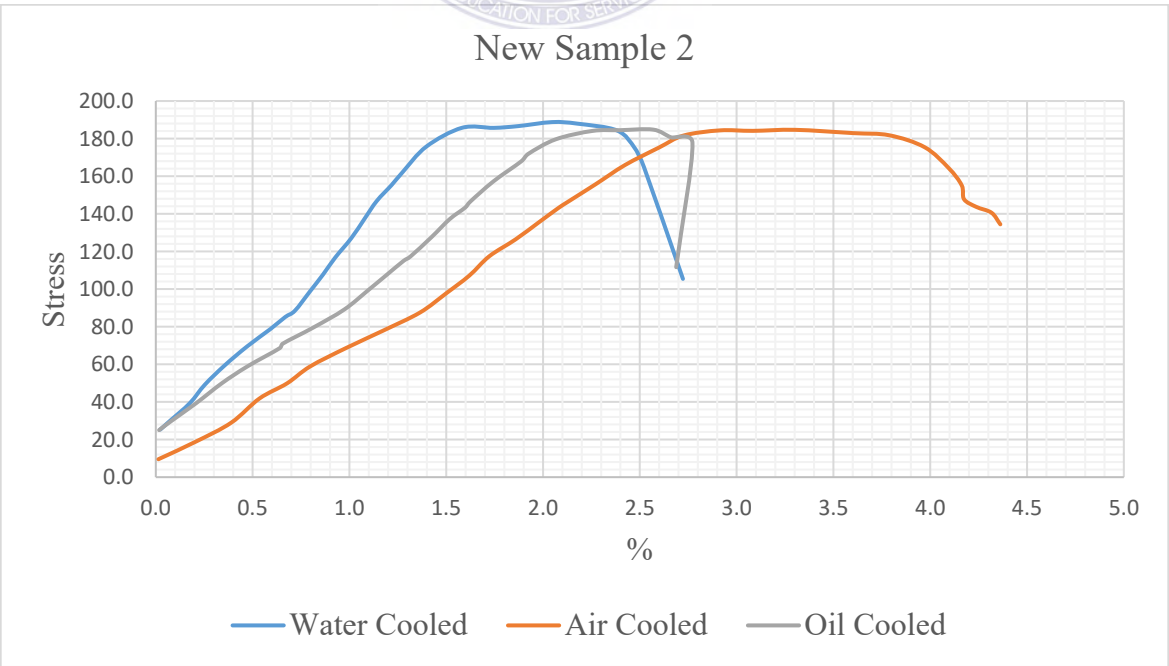

Figure 4. 7 Stress Strain Test for 12mm New Specimen (Water, Air and Oil Cooled), Sample 2

Air Cooled

The Thickness for the specimen was 12, its width was 63.50, with an Area of 762mm^2 and Gauge length of 300. All dimensions are in mm. The Tensile test produced the following outcomes.

Table 4. 5 Outcome of Tensile Test

Description	Value	Unit
Force max	190.293	Kn
Tensile stress Su/Rm	249.7	N/mm^2
Yield stress YS/Rt(.5%)	83.0	N/mm^2
t%	0.5	%
Total elongation EI/ (A)	2.8	%
Young modulus E	11.43	kN/mm^2

Oil Cooled

The Thickness for the specimen was 12, its width was 63.50, with an Area of 762mm^2 and Gauge length of 300. All dimensions are in mm. The Tensile test produced the following outcomes.

Table 4. 6 Outcome of Tensile Test

Description	Value	Unit
Force max	185.599	kN
Tensile stress Su/Rm	243.6	N/mm^2
Yield stress YS/Rt(.5%)	86.1	N/mm^2
t%	0.5	%
Total elongation EI/ (A)	1.5	%
Young modulus E	12.86	kN/mm^2

Water Cooled

The Thickness for the AO1 specimen was 11.8, its width was 25.23, with an Area of 297.71 and Gauge length of 50. All dimensions are in mm.

The Tensile test produced the following outcomes.

Table 4. 7 Outcome of Tensile Test

Description	Value	Unit
Force max	183.311	kN
Tensile stress Su/Rm	253.7	N/mm^2
Yield stress YS/Rt(.5%)	102.2	N/mm^2
t%	0.5	%
Total elongation EI/ (A)	1.9	%
Young modulus E	18.26	kN/mm^2

4.3.1.3 Tensile Test Results for Sample 3 of 12mm New Specimen

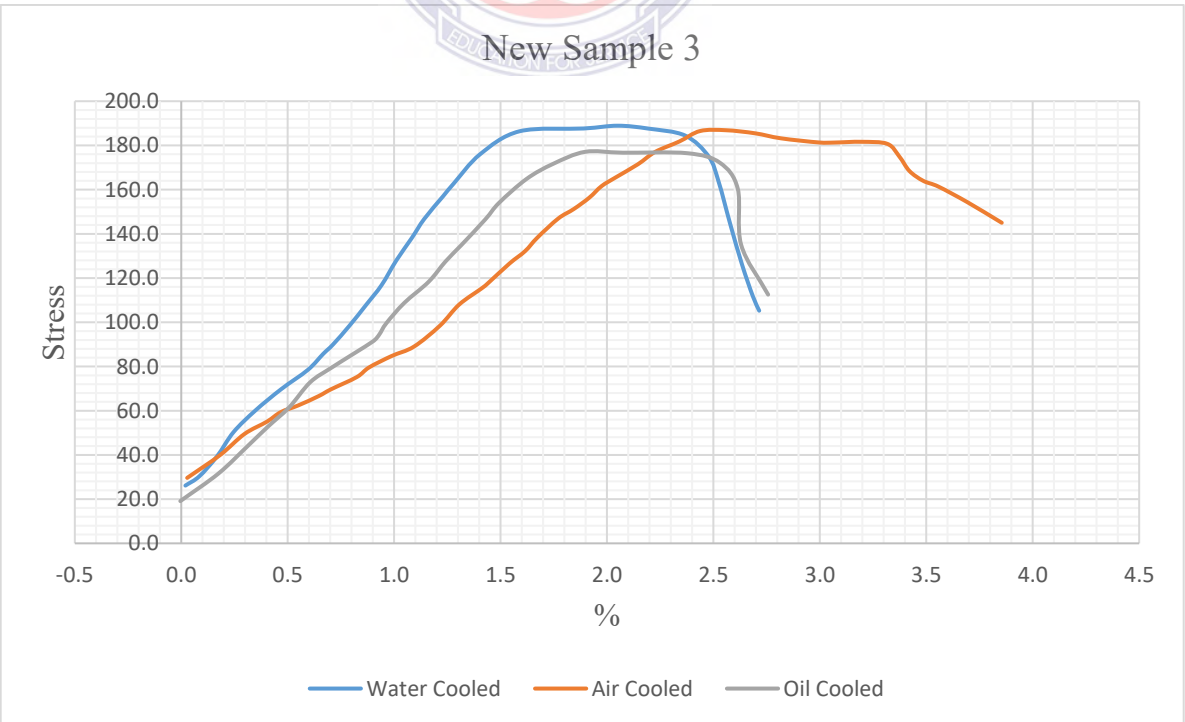

Figure 4. 8 Stress Strain Test for 12mm New Specimen (Water, Air and Oil Cooled), Sample 3

Air Cooled

The Thickness for the specimen was 12, its width was 63.50, with an Area of 762mm^2 and Gauge length of 300. All dimensions are in mm. The Tensile test produced the following outcomes.

Table 4. 8 Outcome of Tensile Test

Description	Value	Unit
Force max	189.284	kN
Tensile stress Su/Rm	248.5	N/mm^2
Yield stress YS/Rt(.5%)	68.1	N/mm^2
t%	0.5	%
Total elongation EI/ (A)	2.6	%
Young modulus E	13.44	kN/mm^2

Oil Cooled

The Thickness for the specimen was 12, its width was 63.50, with an Area of 762mm^2 and Gauge length of 300. All dimensions are in mm. The Tensile test produced the following outcomes.

Table 4. 9 Outcome of Tensile Test

Description	Value	Unit
Force max	194.087	kN
Tensile stress Su/Rm	254.7	N/mm^2
Yield stress YS/Rt(.5%)	86.0	N/mm^2
t%	0.5	%
Total elongation EI/ (A)	1.8	%
Young modulus E	12.78	kN/mm^2

Water Cooled

The Thickness for the specimen was 12, its width was 63.50, with an Area of 762mm^2 and Gauge length of 300. All dimensions are in mm. The Tensile test produced the following outcomes.

Table 4. 10 Outcome of Tensile Test

Description	Value	Unit
Force max	189.782	kN
Tensile stress Su/Rm	249.1	N/mm^2
Yield stress YS/Rt(.5%)	69.7	N/mm^2
t%	0.5	%
Total elongation EI/ (A)	1.4	%
Young modulus E	8.89	kN/mm^2

4.3.2 Tensile Test Results for 12mm Scrap Specimen (Water, Air and Oil Cooled)

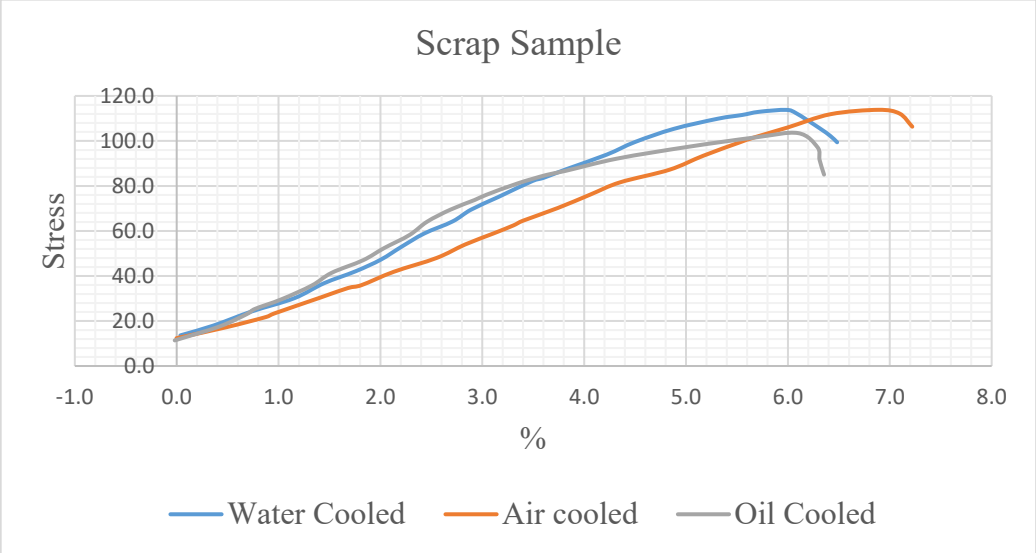

Figure 4. 9 Stress Strain Test for 12mm Scrap Specimen (Water, Air and Oil Cooled)

Air cooled

The Thickness for the specimen was 12, its width was 35.0, with an Area of 420.00mm^2 and Gauge length of 215. All dimensions are in mm. The Tensile test produced the following outcomes.

Table 4. 11 Outcome of Tensile Test

Description	Value	Unit
Force max	116.562	kN
Tensile stress Su/Rm	277.5	N/mm^2
Yield stress YS/Rt(.5%)	43.2	N/mm^2
t%	0.5	%
Total elongation EI/ (A)	1.8	%
Young modulus E	4.72	kN/mm^2

Oil Cooled

The Thickness for the specimen was 12, its width was 35.0, with an Area of 420.00mm^2 and Gauge length of 215. All dimensions are in mm. The Tensile test produced the following outcomes.

Table 4. 12 Outcome of Tensile Test

Description	Value	Unit
Force max	107.876	kN
Tensile stress Su/Rm	256.8	N/mm^2
Yield stress YS/Rt(.5%)	49.3	N/mm^2
t%	0.5	%
Total elongation EI/ (A)	3.2	%
Young modulus E	6.79	kN/mm^2

Water cooled

The Thickness for the specimen was 12, its width was 35.0, with an Area of 420.00mm^2 and Gauge length of 215. All dimensions are in mm. The Tensile test produced the following outcomes.

Table 4. 13 Outcome of Tensile Test

Description	Value	Unit
Force max	116.059	kN
Tensile stress Su/Rm	276.3	N/mm^2
Yield stress YS/Rt(.5%)	47.6	N/mm^2
t%	0.5	%
Total elongation EI/ (A)	2.6	%
Young modulus E	6.05	kN/mm^2

4.3.3.1 Summary of Ultimate Tensile Strength

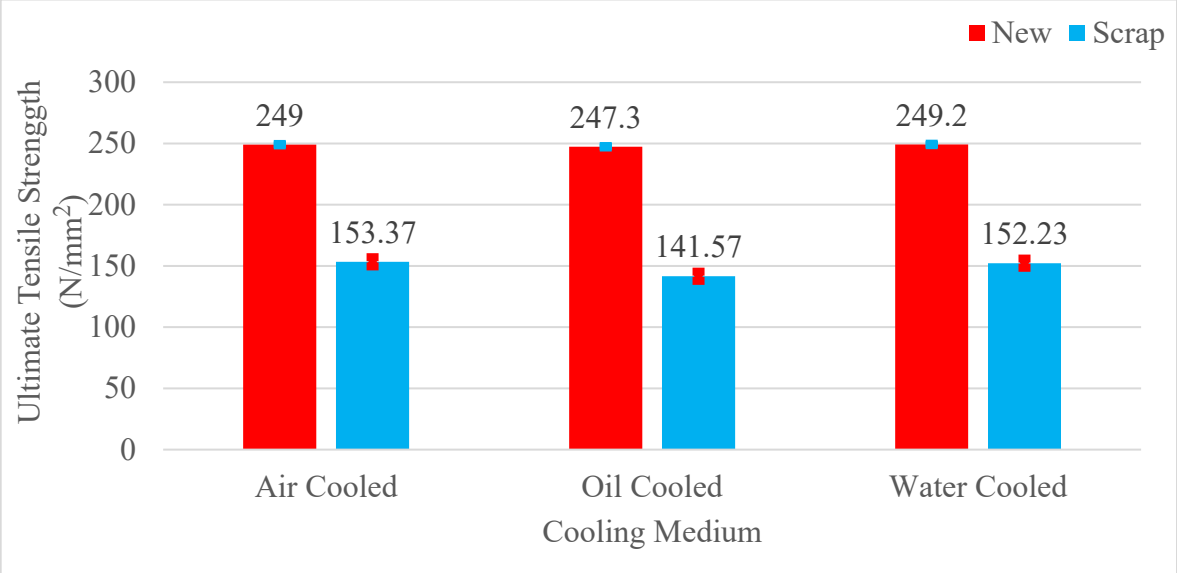

Figure 4. 10 Summary of Tensile Strength of scrap and new heat treated specimen

Fig. 4.9 shows that the water cooled new specimen produces the highest average tensile strength value which is about 249.2. The air and the oil cooled specimen then followed with tensile strength values of 249.0 and 247.3 N/mm^2. However the scrap oil cooled specimen produced the lowest average tensile strength of about 141.57 N/mm^2 follow by the air and water cooled scrap specimen with average tensile strength values of 153.37 and 152.23 respectively. This gives an indication that there is a lower effect of cooling rate on the tensile strength of new carbon steel as compared with scrap carbon steel and this agrees with the conclusions made by Liang (2021) on the effect of cooling rate on microstructure and mechanical properties of a low-carbon low-alloy steel.

4.3.3.2 Summary of Young's Modulus

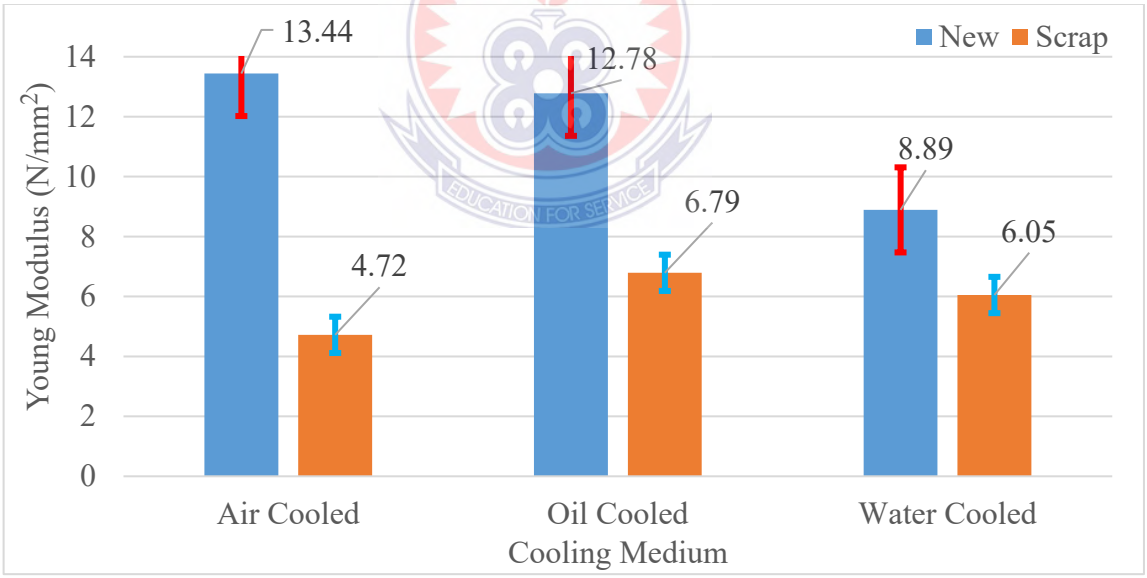

Figure 4. 11 Summary of Young's Modulus of scrap and new heat treated specimen

Fig. 4.10 shows that the water cooled new specimen produces the lowest average young modulus value which is about 8.89 N/mm^2 as compared to the oil and air cooled specimen with average young modulus values of 12.78 and 13.44 N/mm^2. However among the

scrap, the air cooled specimen produced the lowest average young modulus of about 4.72 kN/mm^2 follow by the water and oil cooled scrap specimen with average young modulus values of 6.05 and 6.79 kN/mm^2 respectively. In this case higher young modulus means lower strain levels. This projects that there is a higher effect of cooling rate on the elasticity of scrap low carbon steel as compared with new low carbon steel in consonance with the findings of Liang (2021) on the effect of cooling rate on microstructure and mechanical properties of a low-carbon low-alloy steel.

4.4 IMPACT TEST ANALYSIS

Table 11 and 12 show the results from the impart test and represented in Figs, 26 and 27. The test results were obtained from the digital measuring scale attached to the impact test machine. The machine recorded the impact energy absorbed by the specimen until it failed.

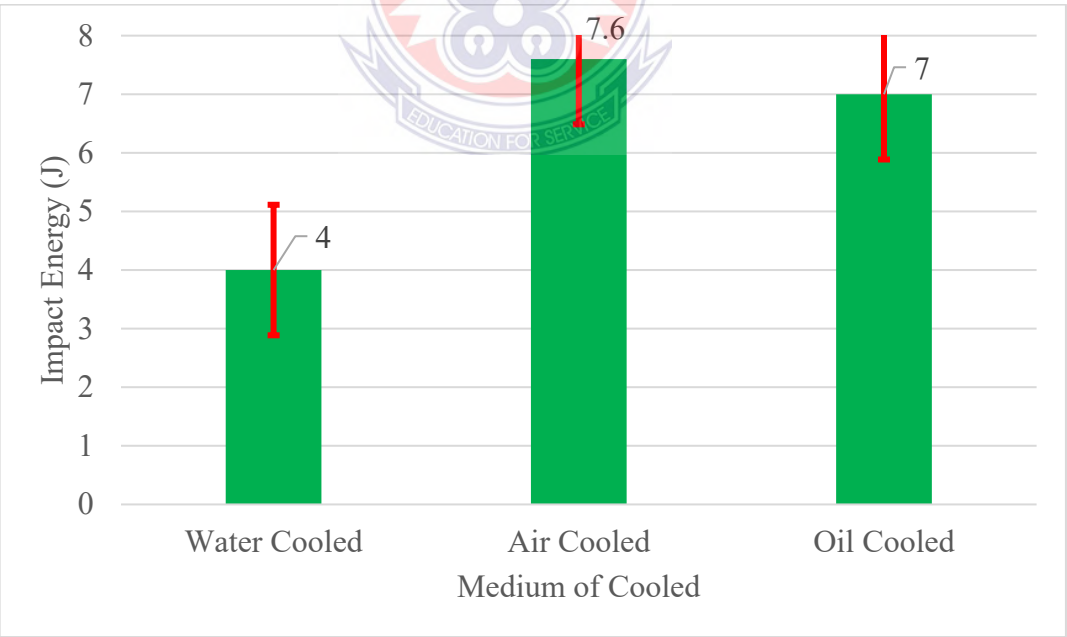

Figure 4. 12 Impart Energy on 12mm New Specimen

From Fig. 4.11, it was observed that the air cooled specimen absorbed more impact energy than both the oil and water cooled specimen. This means that the air cooled specimen is tougher than the oil and water cooled specimen. The difference in the toughness of the air cooled and oil cooled is 7.89% and the difference in the toughness of the air cooled and water cooled is 47.37%.

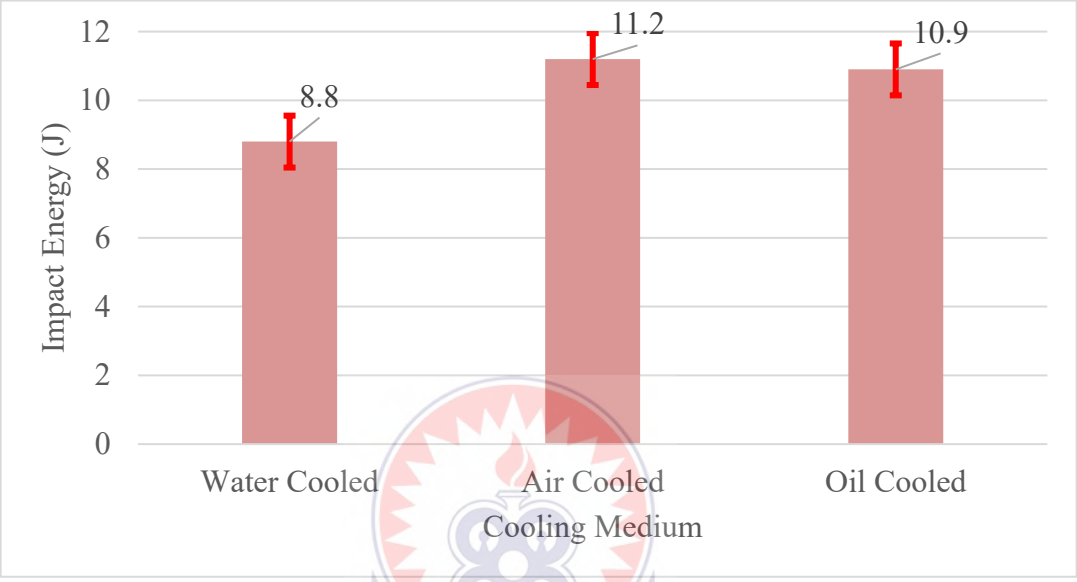

Figure 4. 13 Impart Energy on 12mm Scrap Specimen

From Fig.4.12, it was observed that the air cooled specimen absorbed more impact energy than both the oil and water cooled specimen. This means that the air cooled specimen is tougher than the oil and water cooled specimen. The difference in the toughness of the air cooled and oil cooled is 2.68% and the difference in the toughness of the air cooled and water cooled is 21.43%.

However comparing the new and the scrap specimen, it was observed that the air cooled scrap specimen was tougher than the new specimen with impact energies of 11.2J for the scrap specimen and 7.6J for the new specimen which gives a difference in toughness of 32.14%, the oil cooled scrap specimen was tougher than the new specimen with impact energies of 10.9J or the scrap specimen and 7J for the new specimen which gives a

difference in toughness of 35.78% and the water cooled scrap specimen was tougher than the new specimen with impact energies of 8.8J for the scrap specimen and 4 for the new specimen which gives a difference in toughness of 54.55%. This projects that there is a higher effect of cooling rate on the impact strength of new low carbon steel as compared with scrap low carbon steel which agrees with the findings of Ghosh (2006) on the Effect of cooling rate on structure and properties of an ultra-low carbon steel.

CHAPTER FIVE

SUMMARY OF FINDINGS, CONCLUSION AND RECOMMENDATION

5.1 Introduction

This chapter presents a summary of the main and most significant findings, the conclusions derived from the findings as well as the suggestions and recommendation for further research into the study area.

5.1. Summary of the Main Findings

The summary of the main findings is enumerated as follows;

5.2.1 Main Finding on Hardness

Firstly, the average HV value at the weld zone for the water cooled new specimen was 225.50 as compare to the average HV value at weld zone of 218.50 of the water cooled scrap specimen indicating a hardness difference of 3.10%. At the heat affect zone the average HV values were 229.33 for the new specimen and 224.17 for scrap specimen indicating a hardness difference of 2.25%. Secondly, the average HV value at weld zone for the oil cooled new specimen was 225.17 as compare to the average HV value at weld zone of 212.67 of the oil cooled scrap specimen indicating a hardness difference of 5.55%. At the heat affect zone the average HV values were 190.00 for the new specimen and 157.50 for scrap specimen indicating a hardness difference of 16.97%. Lastly, the average HV value at weld zone for the air cooled new specimen was 225.17 as compare to the average HV value at weld zone of 190.00 of the air cooled scrap specimen indicating a hardness difference of 28.94%. At the heat affect zone the average HV values were 229.50 for the new specimen and 216.67 for scrap specimen indicating a hardness difference of 5.59%.

5.2.2 Main Finding on Ultimate Tensile Strength

The ultimate tensile strength for Air cooled new specimen was 249.00 N/mm^2 as compared to the air cooled scrap specimen which was 153.37 indicating a tensile strength difference of 38.40%. Again, the ultimate tensile strength for oil cooled new specimen was 247.30 N/mm^2 as compared to the oil cooled scrap specimen which was 141.57 N/mm^2 indicating a tensile strength difference of 42.75%. Also, the ultimate tensile strength for water cooled new specimen was 249.20 N/mm^2 as compared to the water cooled scrap specimen which was 152.23 N/mm^2 indicating a tensile strength difference of 38.91%.

5.2.3 Main Finding on Young's Modulus

The Young modulus for the air cooled new specimen was 13.44 kN/mm^2 as compared to the air cooled scrap specimen which was 4.72 kN/mm^2 indicating a young's modulus difference of 64.88%. Also, the young's modulus for the oil cooled new specimen was 12.78 kN/mm^2 as compared to the oil cooled scrap specimen which was 6.79 kN/mm^2 indicating a young's modulus difference of 46.78%. Again, the young's modulus for the water cooled new specimen was 8.89 kN/mm^2 as compared to the water cooled scrap specimen which was 6.05 kN/mm^2 indicating a young's modulus difference of 31.95%.

5.2.4 Main Finding on Impact Energy and Impact Strength

Firstly, The average impact energy for the water cooled new specimen was 4 J with a correspondent impact strength 5.1 J/cm^2 as compared to the water cooled scrap specimen which was 8.8 J with correspondent impact strength 11.0 J/cm^2 indicating an impact energy difference of 54.55% in favour of the scrap specimen. Secondly, the average impact energy for the air cooled new specimen was 7.6 J with a correspondent impact strength 5.1 J/cm^2 as compared to the air cooled scrap specimen which was 11.2 J with correspondent

impact strength 14.0 J/cm^2 indicating an impact energy difference of 32.14% in favour of the scrap specimen. Thirdly, the average impact energy for the oil cooled new specimen was 7.0 J with a correspondent impact strength 9.5 J/cm^2 as compared to the oil cooled scrap specimen which was 10.9 J with correspondent impact strength 13.6 J/cm^2 indicating an impact energy difference of 35.78% in favour of the scrap specimen

5.3 CONCLUSION

From the results obtained and the analysis carried out, it can be concluded that the cooling rate adversely affected the welded joints by the Manual Metal Arc Welding Process, and this also affected the mechanical properties of the low carbon steel metal. Considering the hardness of both new and scrap carbon steel at the weld zone after welding and heat treatment (water cooled, air cooled and oil cooled), the new specimen were harder than the scrap specimen by 3.10%, 5.55% and 28.94% respectively. At the heat affected zone the difference in hardness were 2.25%, 16.97% and 5.59% for water cooled, air cooled and oil cooled specimen respectively.

With the Ultimate Tensile strength, it was observed that the new specimen had higher tensile strength compared to the scrap specimen. The difference in the ultimate tensile strength were 38.91%, 38.40% and 42.75% for water cooled, air cooled and oil cooled respectively.

Also, the study indicated higher elasticity values for the new specimen than the scrap specimen by 31.95%, 64.88% and 46.78% difference in Young's modulus for water cooled, air cooled and oil cooled respectively.

However, it was observed that the scrap specimen had greater impact energy than the new specimen. The difference in the impact energy was recorded as 54.55%, 32.14% and 35.78% for water cooled, air cooled and oil cooled respectively in favour of the scrap specimen.

5.4 RECOMMENDATION

It is recommended that future studies on the effects of cooling rates on mechanical properties of welded joints of low carbon steel should include different scrap metals depending on their longevity so a conclusion could be made on the change in mechanical properties with respect to its longevity.

Also, further research could be carried out on the micro structure before and after welding and heat treatment to ascertain the corrosion rate and other mechanical properties.

It is further recommended that, just like the AISI and ASTM of North America, a regulatory body and standardization body be set up to help streamline and properly regulate the type of low carbon steel scrap used in the mechanical and fabrication industries, to reduce the failure in construction and structural works.

5.5 SUGGESTIONS FOR FURTHER RESEARCH

It is suggested that further research be carried out on equally important industrial material such as plates or rod since this study was only limited to carbon steel plate. It is also suggested that other heat treatment processes be carried out on the sample metal studied to determine their effects on the mechanical properties of the metal.

APPENDIX

Hardness test result

Table 3.5 Hardness Test Results for Water Cooled specimen 12mm New

HARDNESS (HV10)					
1	216	**11**	230	**21**	217
2	217	**12**	235	**22**	233
3	213	**13**	215	**23**	202
4	243	**14**	212	**24**	199
5	243	**15**	215	**25**	217
6	238	**16**	216	**26**	215
7	262	**17**	210	**27**	217
8	220	**18**	207	**28**	212
9	237	**19**	215	**29**	207
10	235	**20**	220	**30**	213

Table 3.6 Hardness Test Results for Water Cooled specimen 12mm Scrap

HARDNESS (HV10)					
1	216	**11**	222	**21**	235
2	215	**12**	220	**22**	215
3	217	**13**	206	**23**	210
4	225	**14**	212	**24**	262

5	228	**15**	213	**25**	220
6	224	**16**	215	**26**	213
7	209	**17**	212	**27**	235
8	209	**18**	217	**28**	233
9	206	**19**	216	**29**	228
10	220	**20**	217	**30**	224

Table 3.7 Hardness Test Results for Air Cooled specimen 12mm new

Point	HV Value	Point	HV Value	Point	HV Value
1	216	**11**	230	**21**	217
2	217	**12**	235	**22**	233
3	213	**13**	215	**23**	202
4	243	**14**	212	**24**	199
5	243	**15**	215	**25**	217
6	238	**16**	216	**26**	215
7	262	**17**	210	**27**	217
8	220	**18**	207	**28**	212
9	237	**19**	215	**29**	207
10	235	**20**	220	**30**	213

Table 3.8 Hardness Test Results for Air Cooled specimen 12mm Scrap

Point	HV Value	Point	HV Value	Point	HV Value
1	213	**11**	228	**21**	199
2	212	**12**	225	**22**	202
3	206	**13**	217	**23**	233
4	220	**14**	215	**24**	217
5	222	**15**	216	**25**	220
6	220	**16**	213	**26**	215
7	206	**17**	207	**27**	207
8	209	**18**	212	**28**	210
9	209	**19**	217	**29**	216
10	224	**20**	215	**30**	215

Table 3.9 Hardness Test Results for oil Cooled specimen 12mm new

Point	HV Value	Point	HV Value	Point	HV Value
1	216	**11**	230	**21**	217
2	217	**12**	235	**22**	233
3	212	**13**	215	**23**	202
4	243	**14**	212	**24**	199
5	244	**15**	215	**25**	217
6	238	**16**	212	**26**	215
7	260	**17**	210	**27**	217
8	220	**18**	207	**28**	212

9	237	**19**	215	**29**	207
10	235	**20**	220	**30**	213

Table 3.10 Hardness Test Results for oil Cooled specimen 12mm scrap

Point	HV Value	Point	HV Value	Point	HV Value
1	220	**11**	190	**21**	212
2	225	**12**	192	**22**	186
3	224	**13**	197	**23**	168
4	220	**14**	199	**24**	170
5	220	**15**	198	**25**	187
6	222	**16**	212	**26**	182
7	205	**17**	212	**27**	187
8	233	**18**	216	**28**	190
9	178	**19**	219	**29**	190
10	193	**20**	207	**30**	194

Impact Test

Table 3.11 Impact Energy and Impact Strength of the 12mm New Specimen

	Water Cooled	Air Cooled	Oil Cooled
Impact Energy(J)	4.0	7.6	7.0
Impact Strength(J/cm^2)	5.1	9.5	5.1

Table 3.12 Impact Energy and Impact Strength of the 12mm Scrap Specimen

	Water Cooled	**Air Cooled**	**Oil Cooled**
Impact Energy(J)	8.8	11.2	10.9
Impact Strength(J/m^2)	11.0	14.0	13.6

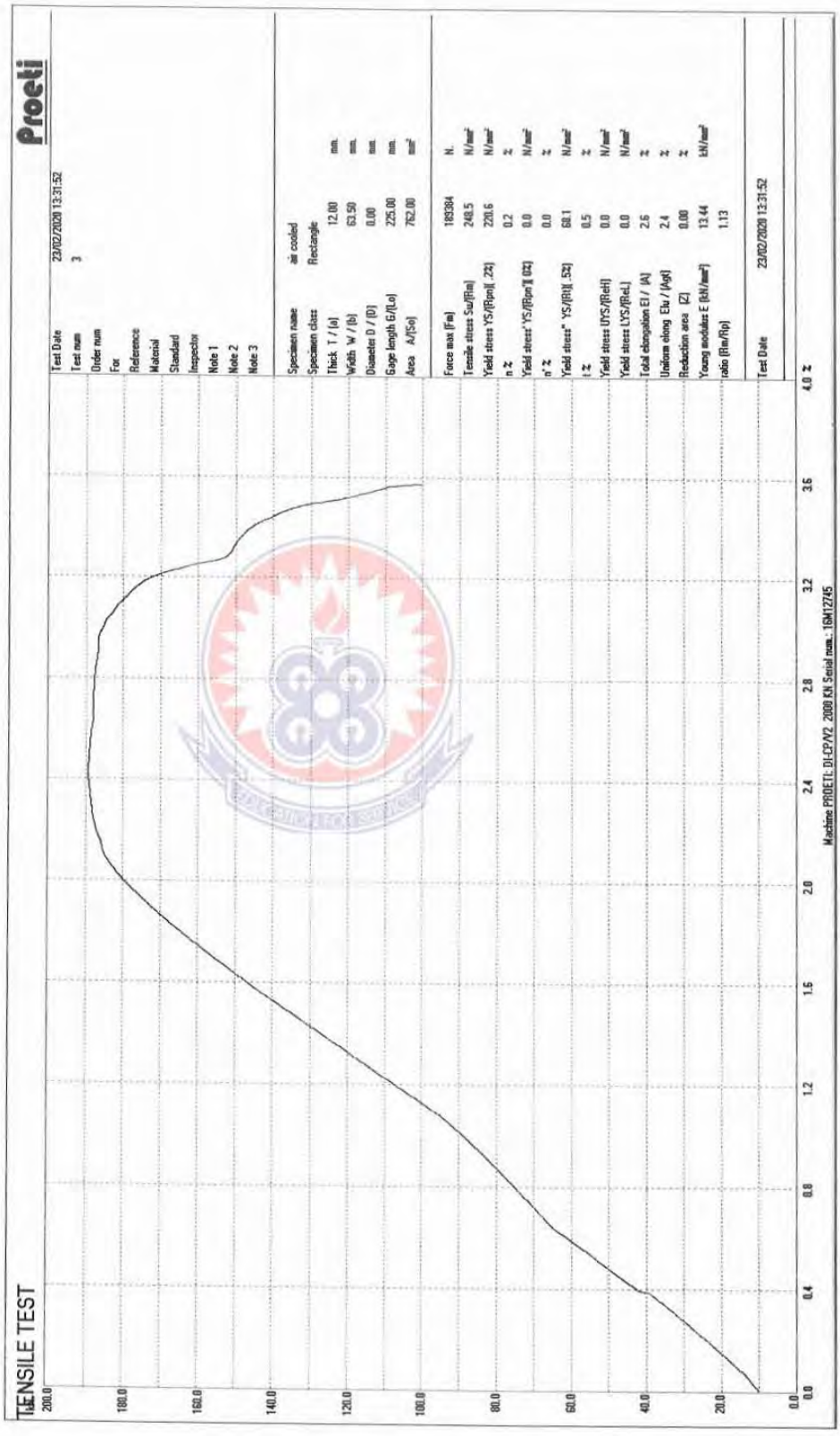

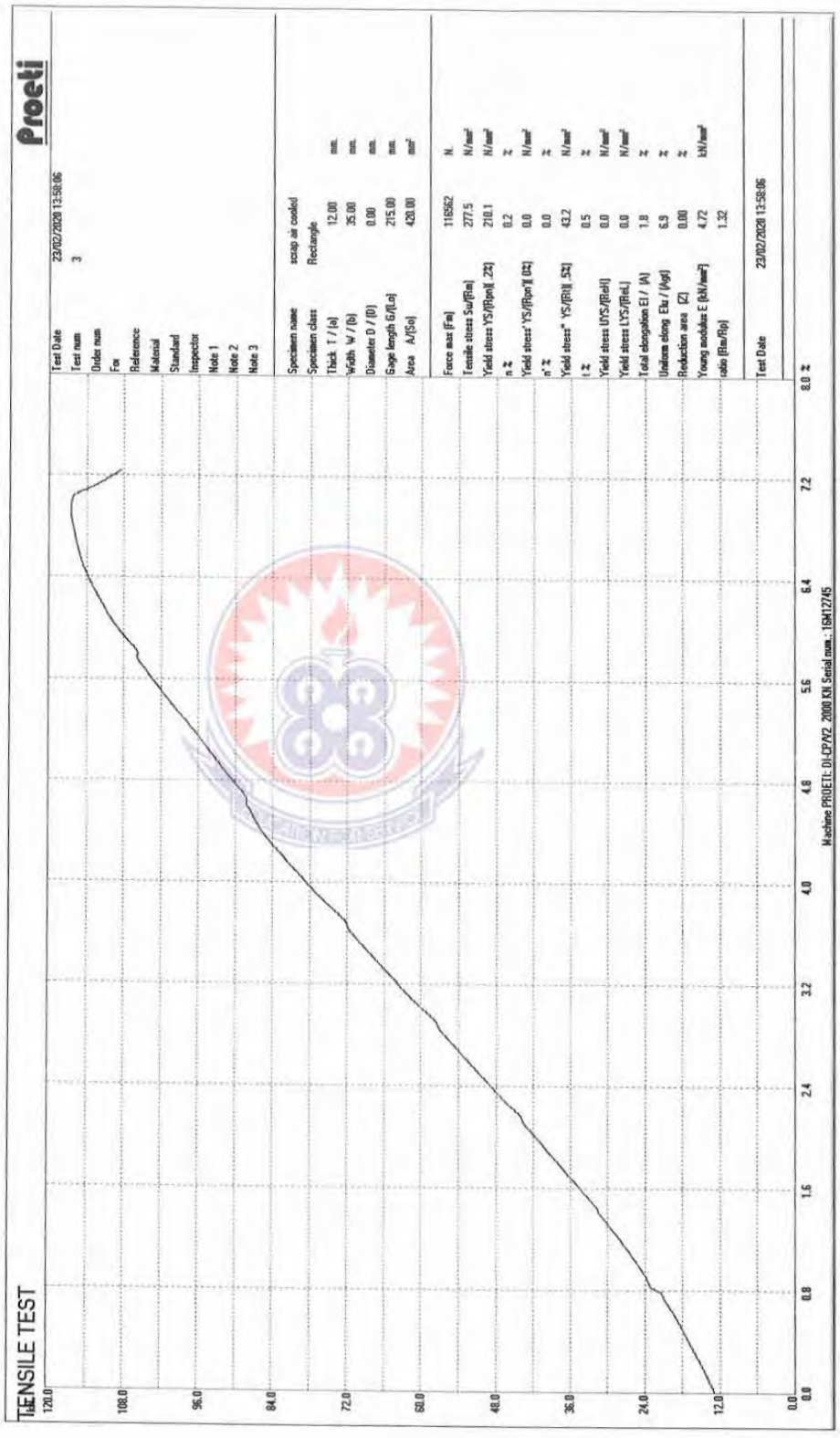

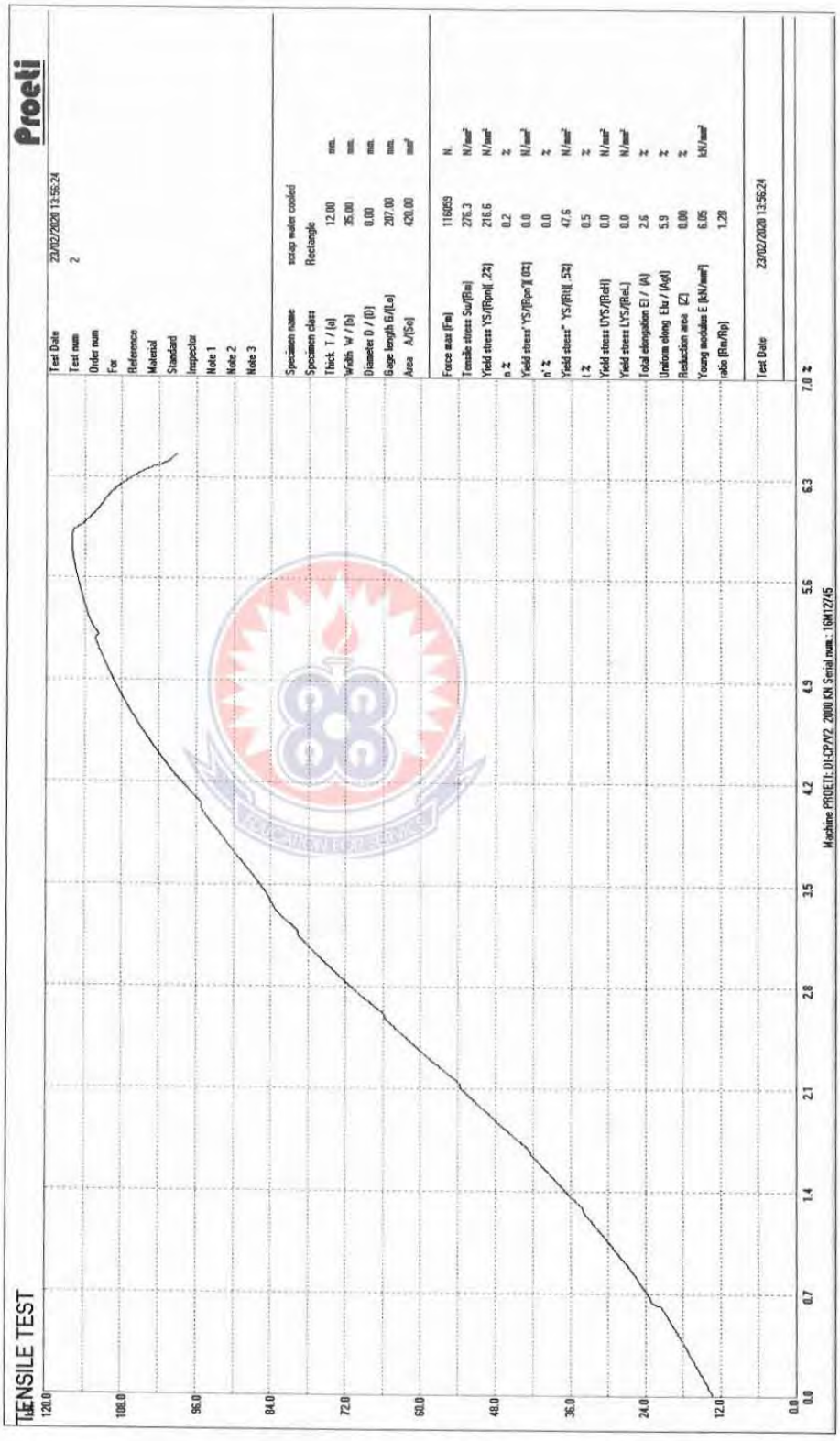

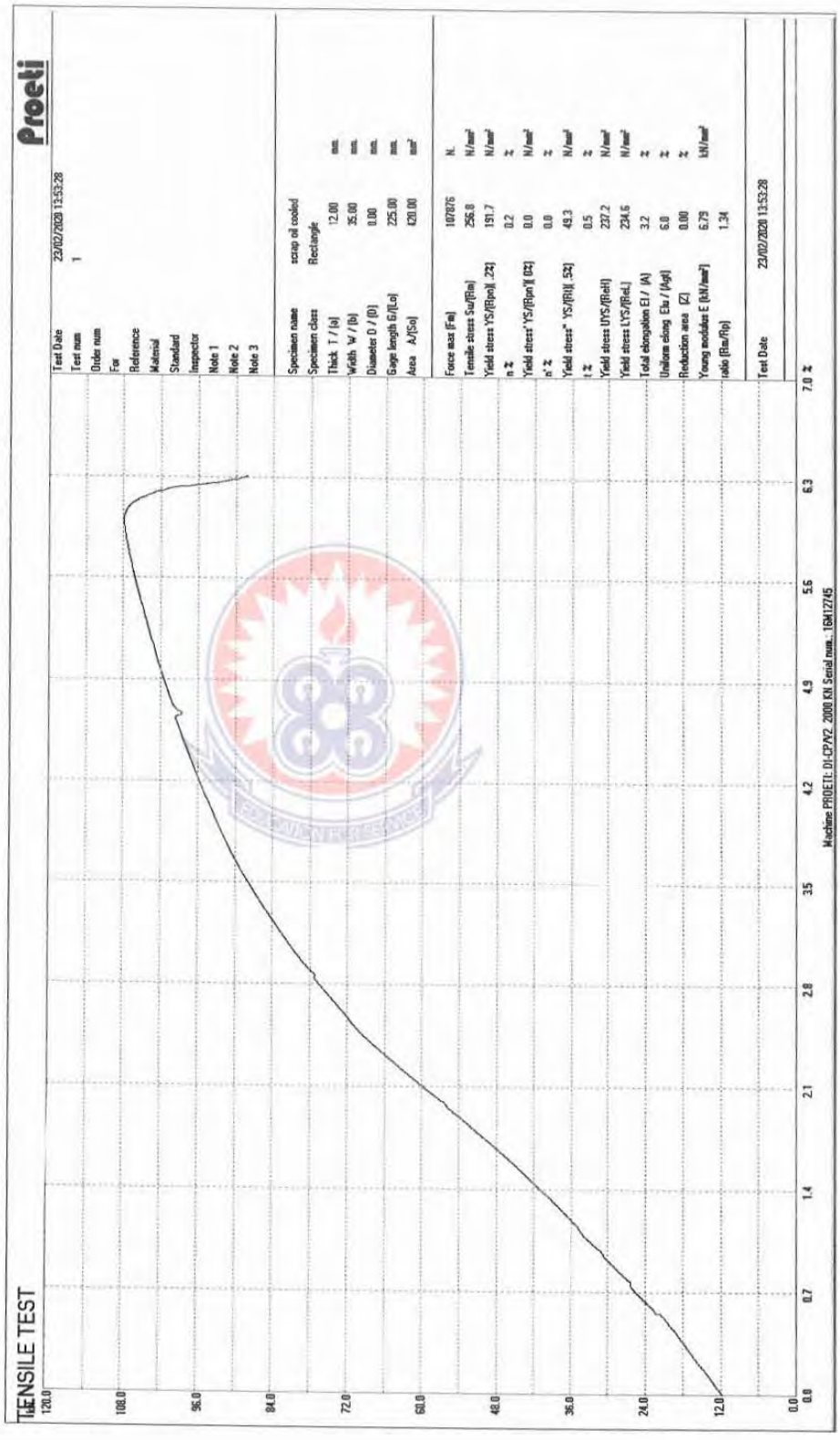

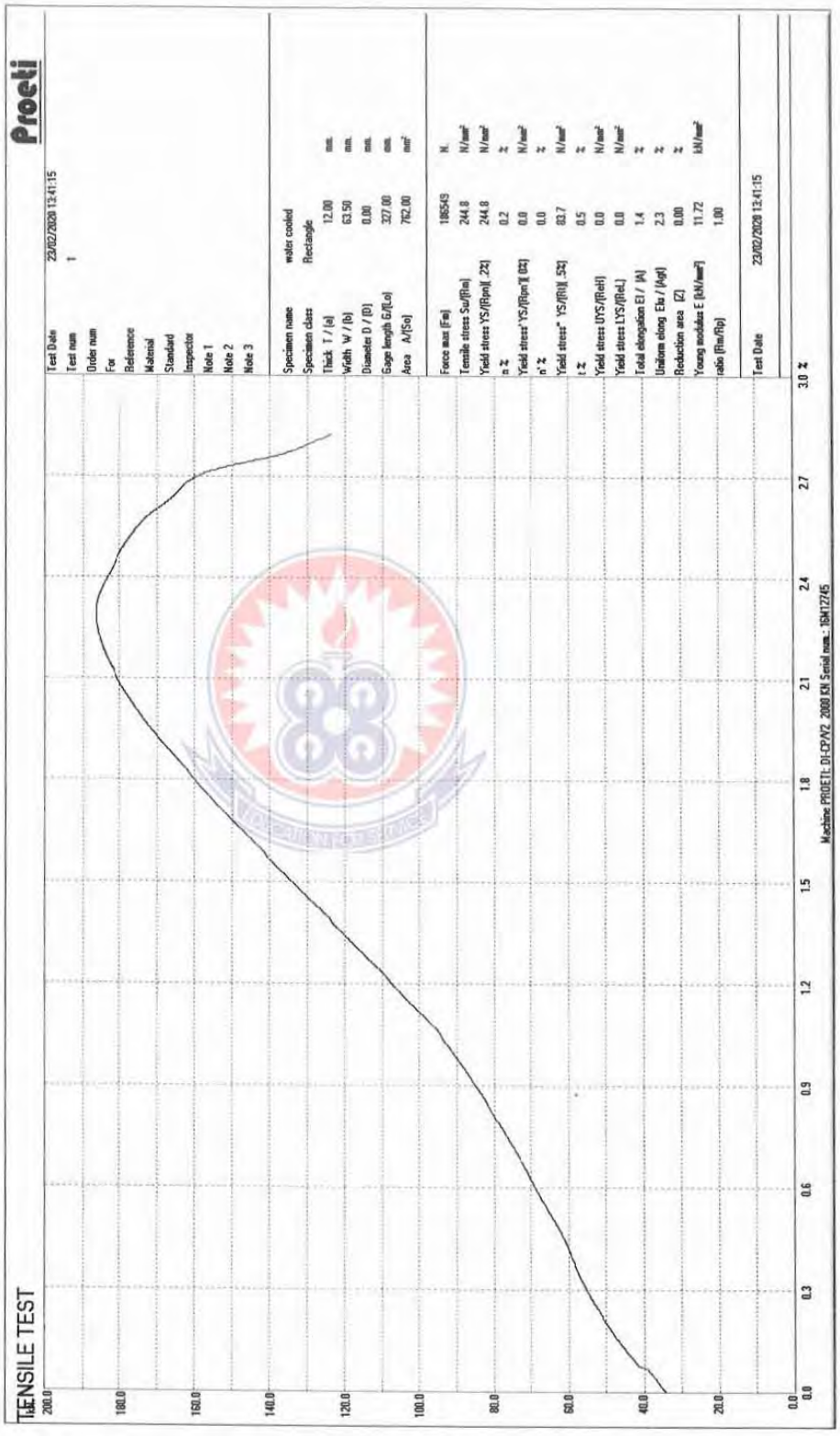

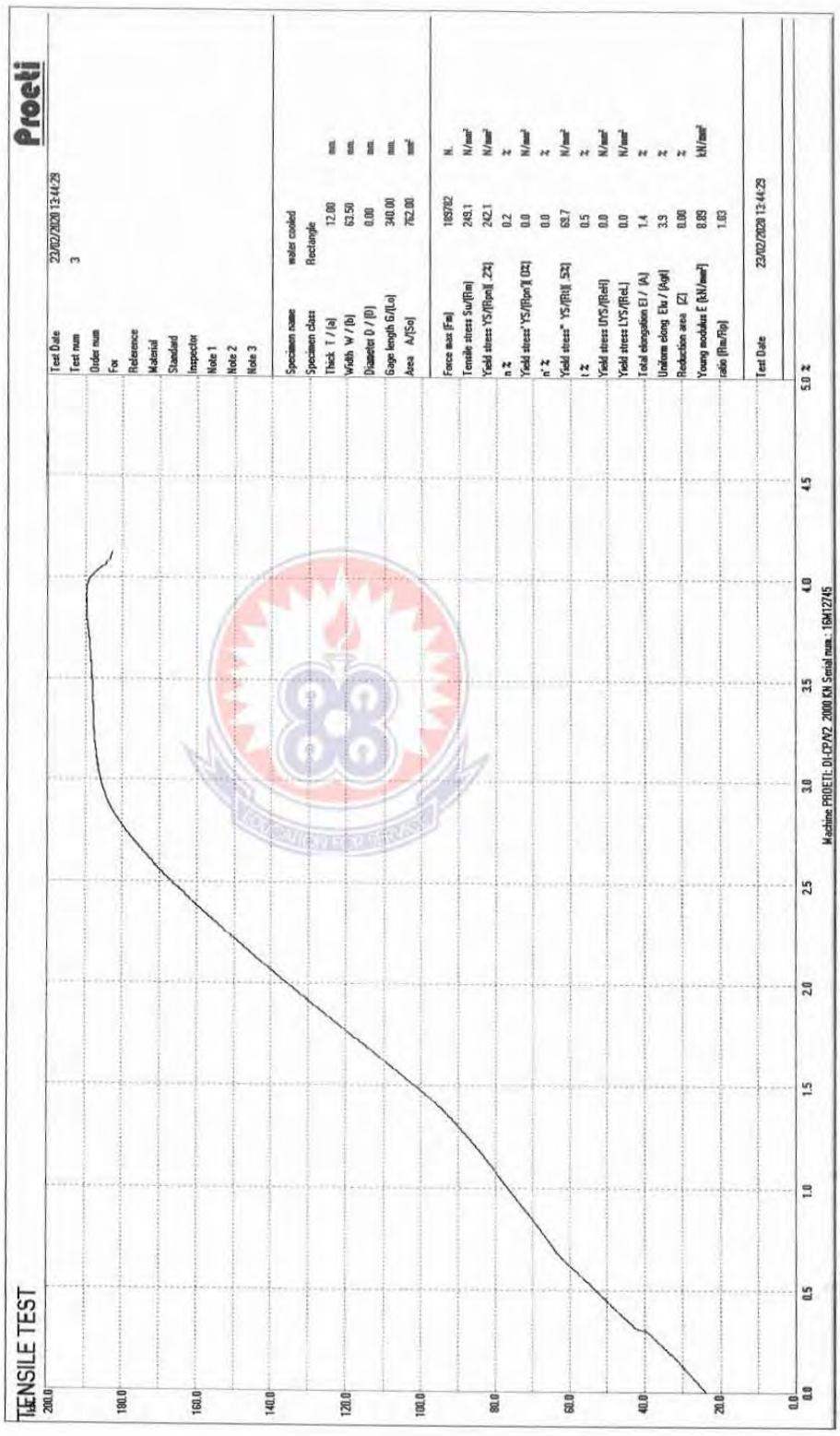

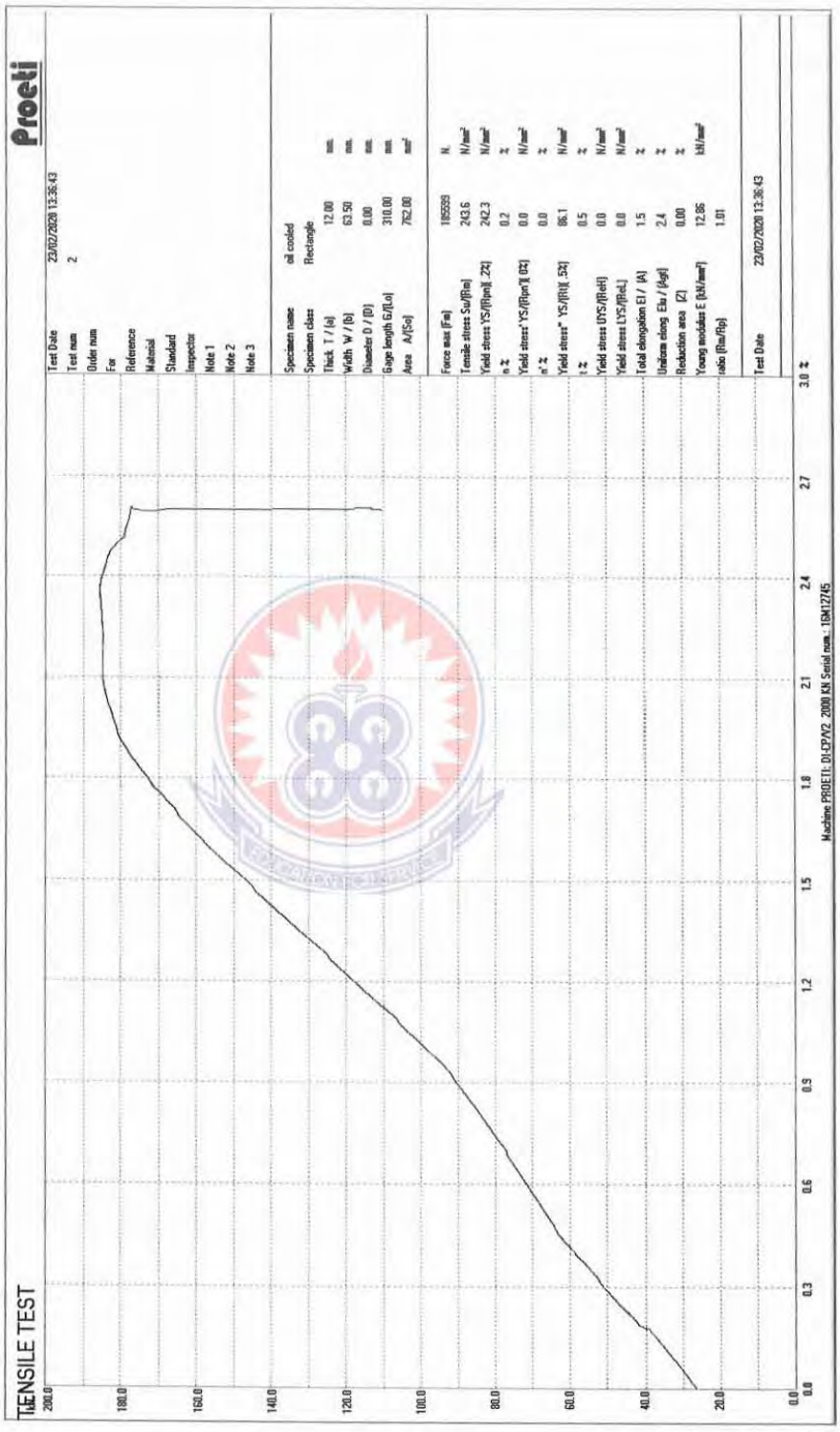

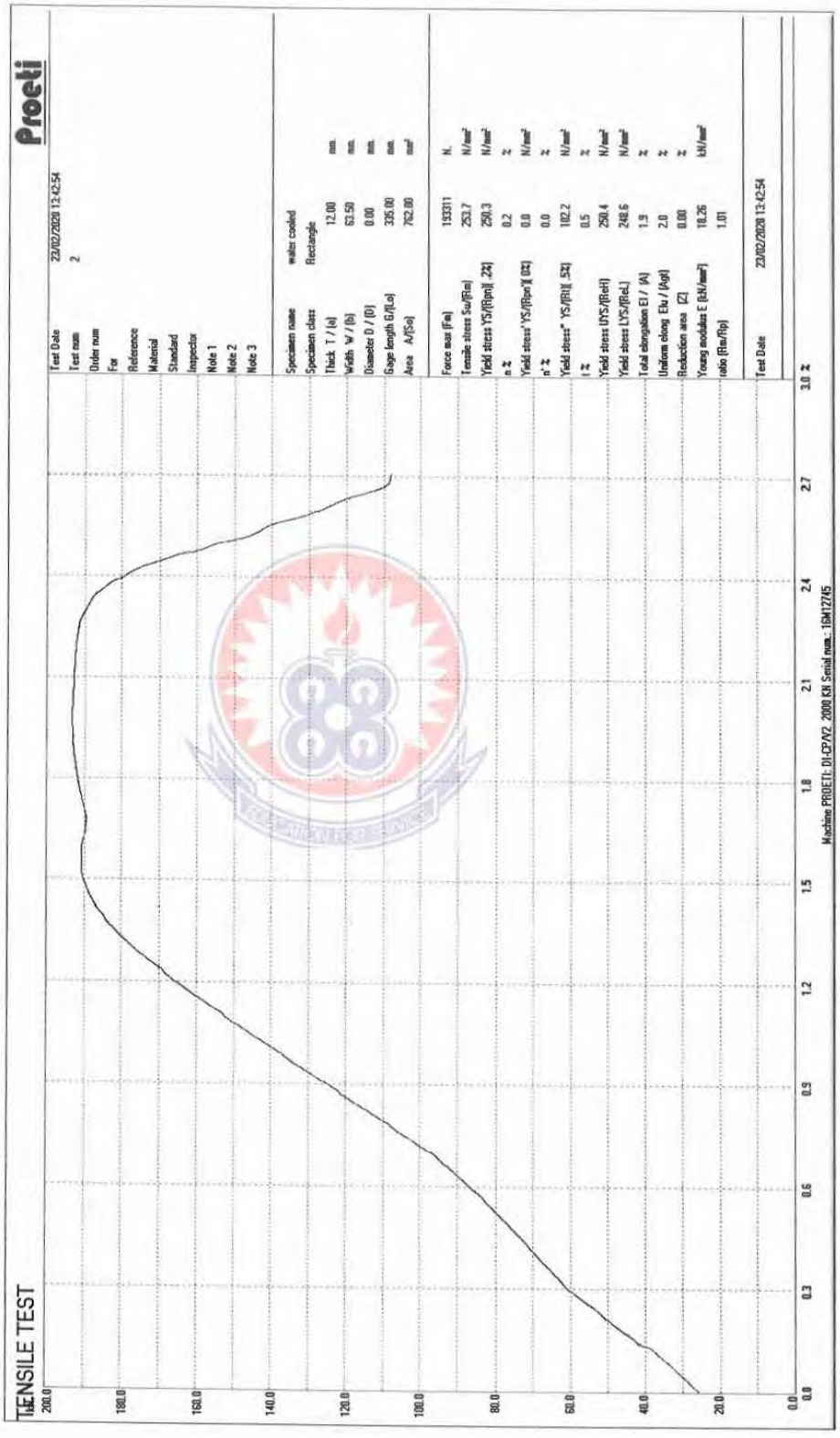

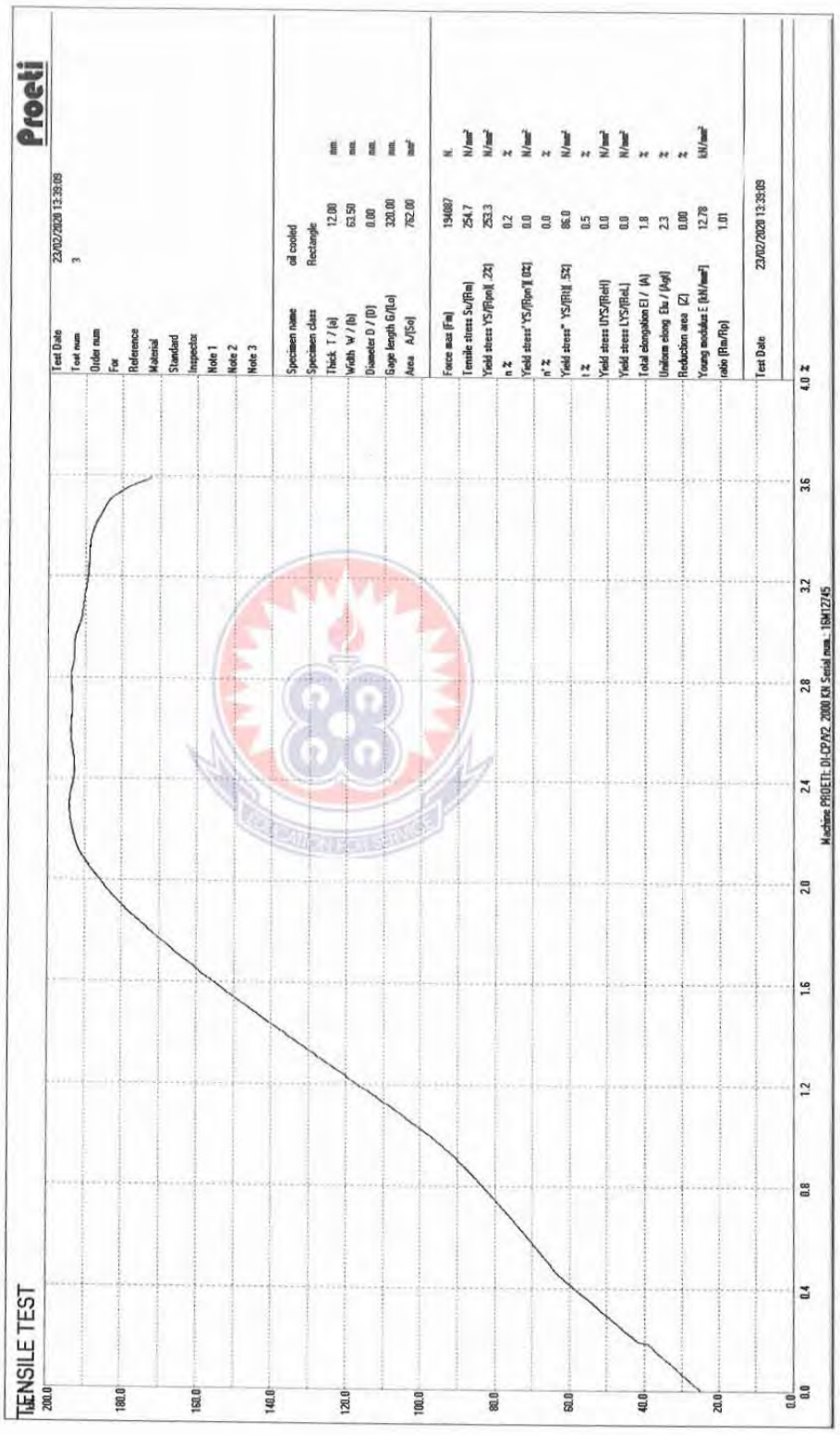

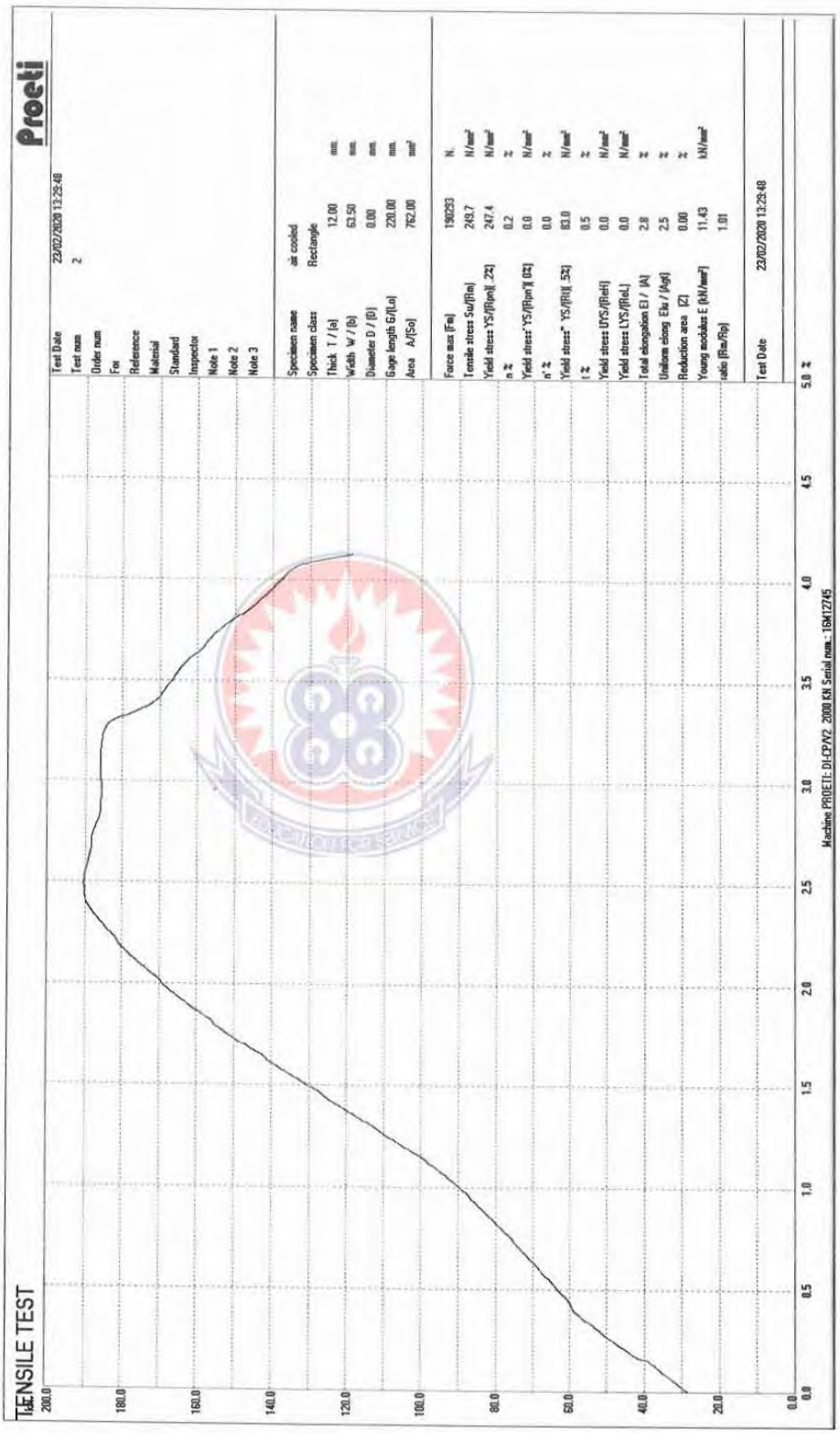

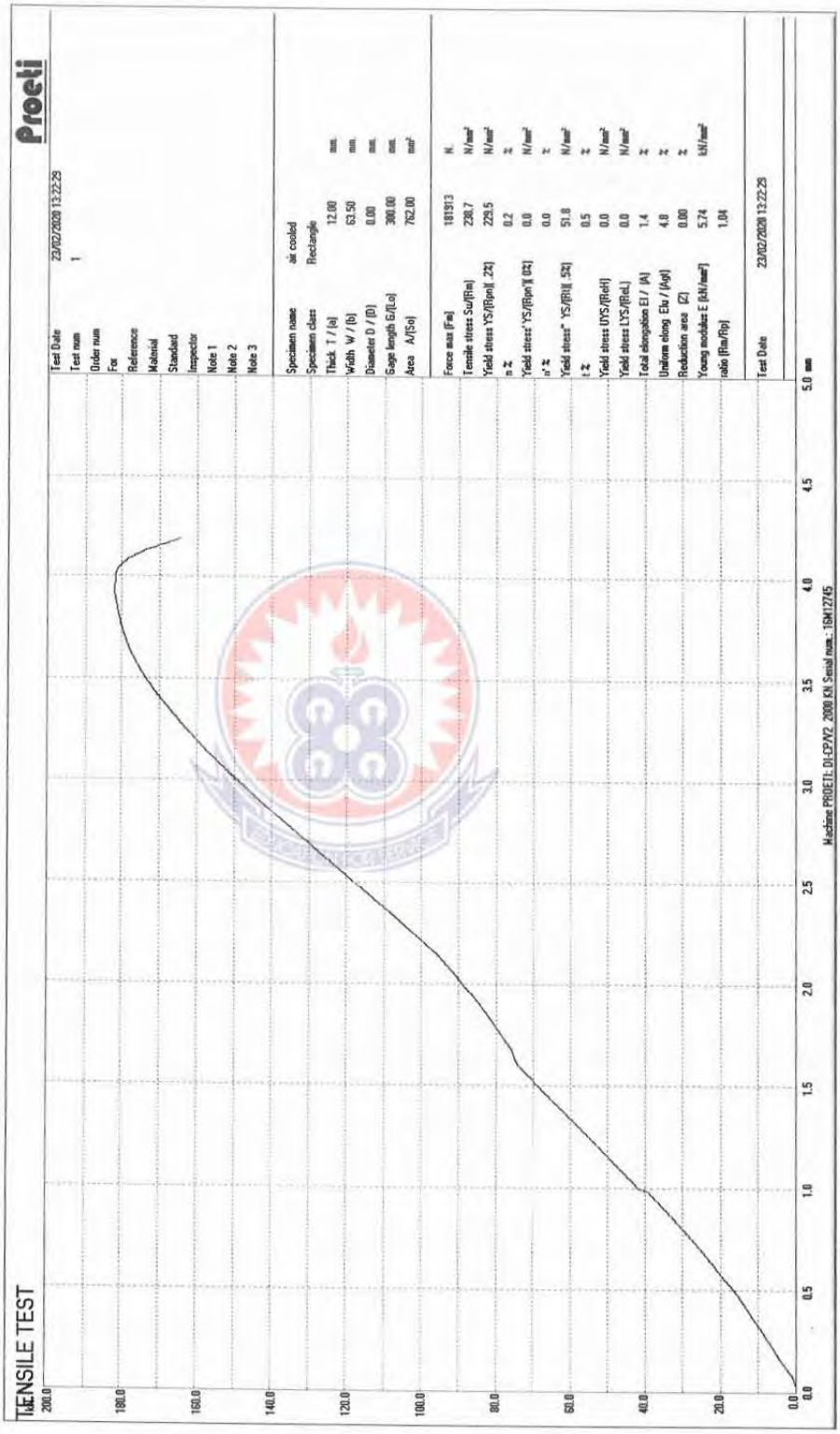

REFERENCES

Ahmad, I., Kano, M., Hasebe, S., Kitada, H., & Murata, N. (2014). Gray-box modeling for prediction and control of molten steel temperature in tundish. *Journal of Process Control, 24(4), 375-382.*

Albano, L. L. M., Kavalco, P. M., Totten, G. E., & Canale, L. C. F. (2012). IFHTSE Global 21: heat treatment and surface engineering in the twenty-first century Part 19–Type I quenchants for quenching of aluminium: a review. *International Heat Treatment and Surface Engineering, 6(4), 146-152.*

Allazadeh, M. R. (2009). *The effect of cooling rate on the microstructure configuration of continuously cast steel slabs* (Doctoral dissertation, University of Pittsburgh).

Allazadeh, M. R. (2010). *Brief history of controlling cooling rate in cast steel.*

Allazadeh, M. R. (2012). Cooling rate optimization of as-cast consciously cast steel. *Iranian Journal of Materials Science and Engineering, 9(3), 1-16.*

Allazadeh, M. R. (2012). Cooling rate optimization of as-cast consciously cast steel. *Iranian Journal of Materials Science and Engineering, 9(3), 1-16.*

Allazadeh, M. R. (2015). *Main Processes in Steel Production with continuously cast Method.*

Amin, M. R., & Mahajan, A. (2002). Effects of Turbulence from Submerged Entry Nozzle During the Solidification Process of Continuous Castings. In *International Heat Transfer Conference Digital Library*. Begel House Inc..

Banerjee, M. K. (2017). 2.1 Fundamentals of Heat Treating Metals and Alloys. *Comprehensive materials finishing*, 1-49.

Bhadeshia, H. K. D. H. (2010). *Phase transformations contributing to the properties of modern steels. Bulletin of the polish academy of sciences.* Technical sciences, 58(2), 255-265.

Boob, A. N., & Gattani, G. K. (2013). *Study on effect of manual metal Arc welding process parameters on width of heat affected zone (HAZ) for Ms 1005 steel. Int. J. Mod*. Eng. Res., 3(3), 1493-1500.

Broadbent, C. (2016). Steel's recyclability: demonstrating the benefits of recycling steel to achieve a circular economy. *The International Journal of Life Cycle Assessment, 21(11), 1658-1665.*

Calcagnotto, M., Adachi, Y., Ponge, D., & Raabe, D. (2011). *Deformation and fracture mechanisms in fine-and ultrafine-grained ferrite/martensite dual-phase steels and the effect of aging.* Acta Materialia, 59(2), 658-670.

Cary, H. B., & Helzer, S. C. *Modern welding technology, 2005.*

Chryssolouris, G. (2013) *Manufacturing systems: theory and practice. Springer Science & Business Media.*

Dewangan, S., Behera, S., & Chowrasia, M. K. (2020). Comparative analysis into mechanical properties and microstructural attributes of quenched and tempered 0.2%-C steel. World Journal of Engineering.

Dossett, J., & Totten, G. E. (2014). Quenchant Agitation, Design, and Characterization.

Evans, G. M. (1982). The effect of heat input on the microstructure and properties of C--Mn all-weld-metal deposits. *Welding Journal*, *61*(4), 125.

Ferng, Y. M., Chieng, C. C., & Pan, C. (1989). Numerical simulations of electro-slag remelting process. *Numerical heat transfer*, *16*(4), 429-449.

Ge, J., Lin, J., Lei, Y., & Fu, H. (2018). Location-related thermal history, microstructure, and mechanical properties of arc additively manufactured 2Cr13 steel using cold metal transfer welding. Materials Science and Engineering: A, 715, 144-153.

Ghosh, A., Das, S., Chatterjee, S., & Rao, P. R. (2006). Effect of cooling rate on structure and properties of an ultra-low carbon HSLA-100 grade steel. *Materials Characterization*, *56*(1), 59-65.

Greif, D. (1998). Numerical study of conjugate heat transfer in a continuously moving metal during solidification (Doctoral dissertation, Montana State University-Bozeman, College of Engineering).

Gyasi, E. A., Kah, P., & Martikainen, J. (2014). Welding management as a tool for innovative, competitive and sustainable manufacturing: Case study–West Africa. *Int. J. Dev. Sustain.*, *3*, 1782-93.

Hömberg, D., Liu, Q., Montalvo-Urquizo, J., Nadolski, D., Petzold, T., Schmidt, A., & Schulz, A. (2016). Simulation of multi-frequency-induction-hardening including phase transitions and mechanical effects. Finite Elements in Analysis and Design, 121, 86-100.

Huang, X., Thomas, B. G., & Najjar, F. M. (1992). Modeling superheat removal during continuous casting of steel slabs. *Metallurgical and Materials Transactions B*, *23*(3), 339-356.

Jaluria, Y., & Himasekhar, K. (1983). Buoyancy-induced two-dimensional vertical flows in a thermally stratified environment. *Computers & Fluids*, *11*(1), 39-49.

Kang, B. H., & Jaluria, Y. (1993). Thermal modeling of the continuous casting process. *Journal of thermophysics and heat transfer*, *7*(1), 139-147.

Kou, S. (1981). Simulation of heat flow during the welding of thin plates. Metallurgical Transactions A, 12(12), 2025-2030.

Kuziak, R., Kawalla, R., & Waengler, S. (2008). Advanced high strength steels for automotive industry. Archives of civil and mechanical engineering, 8(2), 103-117.

Lee, H. S., Murthy, S. S., Haider, S. W., & Morse, D. V. (1996). Primary production scheduling at steelmaking industries. *IBM Journal of Research and Development*, *40*(2), 231-252.

Lee, S. L., & Tzong, R. Y. (1995). Latent heat method for solidification process of a binary alloy system. *International journal of heat and mass transfer*, *38*(7), 1237-1247.

Liang, G., Tan, Q., Liu, Y., Wu, T., Yang, X., Tian, Z., ... & Zhang, M. X. (2021). Effect of cooling rate on microstructure and mechanical properties of a low-carbon low-alloy steel. *Journal of Materials Science*, *56*(5), 3995-4005.

Lippold, J. C., Kiser, S. D., & DuPont, J. N. (2011). *Welding metallurgy and weldability of nickel-base alloys*. John Wiley & Sons.

Mahapatra, R. B., Brimacombe, J. K., & Samarasekera, I. V. (1991). Mold behavior and its influence on quality in the continuous casting of steel slabs: Part II. Mold heat transfer, mold flux behavior, formation of oscillation marks, longitudinal off-corner depressions, and subsurface cracks. *Metallurgical and Materials Transactions B*, *22*(6), 875-888.

McDaniel, D. J., & Zabaras, N. (1994). A least-squares front-tracking finite element method analysis of phase change with natural convection. *International Journal for Numerical Methods in Engineering*, *37*(16), 2755-2777.

Meirmanov, A. M. (2011). The Stefan Problem (Vol. 3). Walter de Gruyter.

Nakato, H., Ozawa, M., Kinoshita, K., Habu, Y., & Emi, T. (1981). Factors Affecting the Formation of Shell and Longitudinal Cracks in Mold during High Speed Continuous Casting of Slabs. *Tetsu-to-Hagané*, *67*(8), 1200-1209.

Nonino, C., Del Giudice, S., & Savino, S. (2006). Temperature dependent viscosity effects on laminar forced convection in the entrance region of straight ducts. *International journal of heat and mass transfer*, *49*(23-24), 4469-4481.

Pauliuk, S., Kondo, Y., Nakamura, S., & Nakajima, K. (2017). Regional distribution and losses of end-of-life steel throughout multiple product life cycles—Insights from the global multiregional MaTrace model. Resources, Conservation and Recycling, 116, 84-93.

Pedišić, L., Matijević, B., & NOVINA, B. (2014). Quenching oil selection based on tribological effects at metal cooling processes. In Proceeding of the 8th Int. Conference on Tribology BALKANTRIB'14Sinaia, Romania (pp. 376-383).

Petrus, B., Bentsman, J., & Thomas, B. G. (2010). Feedback control of the two-phase Stefan problem, with an application to the continuous casting of steel. In *49th IEEE Conference on Decision and Control (CDC),* IEEE.

Proell, S. D., Wall, W. A., & Meier, C. (2020). On phase change and latent heat models in metal additive manufacturing process simulation. *Advanced Modeling and Simulation in Engineering Sciences*, *7*, 1-32.

Ramesh, G., & Narayan Prabhu, K. (2014). Effect of thermal conductivity and viscosity on cooling performance of liquid quench media. International Heat Treatment and Surface Engineering, 8(1), 24-28.

Rana, A. K., & Dey, P. P. (2021). Predicting Plastic Flow Behaviour, Failure Mechanisms and Severe Deformation Localisation of Dual-Phase Steel using RVE Simulation. International Journal of Automotive and Mechanical Engineering, 18(1), 8601-8611.

Ratnayake, R. C. (2013). An algorithm to prioritize welding quality deterioration factors: A case study from a piping component fabrication process. *International Journal of Quality & Reliability Management*.

Ray, A., & CHAKRABARTI, D. (2011). Cleavage Initiation in Steel: Competition between Large Grains and Large Particles. Indian Institute of Technology Kharagpur.

Reti, T., Fried, Z., & Felde, I. (2001). Computer simulation of steel quenching process using a multi-phase transformation model. Computational Materials Science, 22(3-4), 261-278.

Sarkar, J., Modak, P., Singh, S. B., & Chakrabarti, D. (2021). Effect of cooling-rate during solidification on the structure-property relationship of hot deformed low-carbon steel. Materials Chemistry and Physics, 257, 123826.

Sherby, O. D., Wadsworth, J., Lesuer, D. R., & Syn, C. K. (2008). Revisiting the structure of martensite in iron-carbon steels. Materials transactions, 49(9), 2016-2027.

Sighinolfi, D., & Paganelli, M. (2011, October). Study of the behaviour of mould powders for continuous casting by using the heating microscope. In IOP Conference Series: Materials Science and Engineering (Vol. 18, No. 22, p. 222007). IOP Publishing.

Symeonidis, K., Apelian, D., & Makhlouf, M. M. (2009). The Controlled Diffusion Solidification Process--Fundamentals and Principles (Doctoral dissertation, Worcester Polytechnic Institute).

Totten, G. E., Xie, L., & Funatani, K. (2003). *Handbook of mechanical alloy design* (Vol. 164). CRC press.

Wolff, F., & Viskanta, R. (1988). Solidification of a pure metal at a vertical wall in the presence of liquid superheat. *International journal of heat and mass transfer*, *31*(8), 1735-1744.

Worrell, E., & Reuter, M. (Eds.). (2014). *Handbook of Recycling: State-of-the-art for Practitioners, Analysts, and Scientists*. Newnes.

Xin, R. S., Ma, Q. X., & Li, W. Q. (2017). Effect of heat treatment on microstructure and hardness of internal crack healing in a low carbon steel. In *Key Engineering Materials*. Trans Tech Publications Ltd.

Xu, Q., Zhu, C. F., Zheng, L. W., & Yin, Y. R. (2011). Molten steel breakout prediction based on thermal friction measurement. Journal of Iron and Steel Research, International, 18(4), 24-35.

Yan, C., Hao, L., Hussein, A., Young, P., Huang, J., & Zhu, W. (2015). Microstructure and mechanical properties of aluminium alloy cellular lattice structures manufactured by direct metal laser sintering. Materials Science and Engineering: A, 628, 238-246.

Zhong, H. G., Chen, X. R., Liu, Y. J., Wei, Z. Q., Yu, H. F., & Zhai, Q. J. (2021). Influences of superheat and cooling intensity on macrostructure and macrosegregation of duplex stainless steel studied by thermal simulation. Journal of Iron and Steel Research International, 1-8.